Thesis for the degree of Doctor of Philosophy

Multilevel modulation in short-range optical links

Krzysztof Szczerba

Multilevel modulation in short-range optical links

Krzysztof Szczerba

Front cover illustration: An eye diagram of 60 Gbps 4-PAM after transmission over a few meters of multimode fiber.

Multilevel modulation in short-range optical links

Krzysztof Szczerba

Photonics Laboratory
Department of Microtechnology and Nanoscience (MC2)
Chalmers University of Technology, SE-412 96 Göteborg, Sweden

Abstract

Power and cost efficient short-range optical links are one of the technologies enabling large scale high-performance computers and data centers. Such links typically use directly modulated vertical cavity surface emitting lasers, multi-mode fiber, direct detection and on-off keying (OOK) modulation. In this work replacement of OOK with multilevel modulation formats is studied, with possible application in future optical interconnects.

Subcarrier modulation and pulse amplitude modulation (PAM) were studied because they can be implemented in systems using intensity modulation and direct detection. Previously known subcarrier modulation formats were found to use the optical power inefficiently. In this thesis optimized subcarrier formats were demonstrated experimentally, in particular a three-dimensional four-level optimized subcarrier format called on-off phase-shift keying with 0.6 dB sensitivity improvement over OOK and 2 dB improvement over subcarrier quadrature phase shift-keying at the same bit rate. Similar sensitivity improvements were demonstrated for eight- and sixteen-level subcarrier formats.

PAM offers a good trade-off between complexity and sensitivity. It was demonstrated in real-time at bit-rates of up to 60 Gbps with four levels and up to 35 Gbps with eight levels. Practical aspects of its implementation, such as robustness to intersymbol interference and application of forward error correction (FEC) were investigated theoretically and experimentally. It was shown that 4-PAM with FEC can double the throughput relative to OOK in the same system, while retaining similar sensitivity.

Keywords: intensity modulation, direct detection, pulse amplitude modulation, subcarrier modulation, multi-dimensional modulation formats, sensitivity optimization, VCSEL, multi-mode fibre

List of Papers

This thesis is based on the following appended papers:

[A] K. Szczerba, B.-E. Olsson, P. Westbergh, A. Rhodin, J. S. Gustavsson, Å. Haglund, M. Karlsson, A. Larsson and P. A. Andrekson, "37 Gbps transmission over 200 m of MMF using single cycle subcarrier modulation and a VCSEL with 20 GHz modulation bandwidth," in Proceedings of the *36th European Conference on Optical Communications*, Turin, Italy, Sept. 2010, paper We.7.B.2.

[B] K. Szczerba, J. Karout, P. Westbergh, E. Agrell, M. Karlsson, P. A. Andrekson, and A. Larsson, "Experimental comparison of modulation formats in IM/DD links," *Optics Express*, vol. 19, no. 10, pp. 9881–9889, May 2011.

[C] K. Szczerba, J. Karout, E. Agrell, P. Westbergh, M. Karlsson, P. A. Andrekson, and A. Larsson, "Demonstration of 8-level subcarrier modulation sensitivity improvement in an IM/DD system," in Proceedings of the *37th European Conference on Optical Communications*, Geneva, Switzerland, Sept. 2011, paper We.10.P1.117.

[D] K. Szczerba, J. Karout, M. Karlsson, P. A. Andrekson, and E. Agrell, "Optimized lattice-based 16-level subcarrier modulation for IM/DD systems," in Proceedings of the *38th European Conference on Optical Communication*, Amsterdam, Netherlands, Sept. 2012, paper Mo.1.B.4.

[E] K. Szczerba, P. Westbergh, J. Karout, J. S. Gustavsson, Å. Haglund, M. Karlsson, P. A. Andrekson, E. Agrell, and A. Larsson, "30 Gbps 4-PAM transmission over 200 m of MMF using an 850 nm VCSEL," *Optics Express*, vol. 19, no. 26, pp. B203–B208, Nov. 2011.

[F] K. Szczerba, P. Westbergh, J. Karout, J. S. Gustavsson, Å. Haglund, M. Karlsson, P. A. Andrekson, E. Agrell, and A. Larsson, "4-PAM for high-speed short-range optical communications," *Journal of Optical Communications and Networking*, vol. 19, no. 11, pp. 885–894, Jul. 2012.

[G] K. Szczerba, P. Westbergh, E. Agrell, M. Karlsson, P. A. Andrekson, and A. Larsson, "Comparison of intersymbol interference power penalties for OOK and 4-PAM in short-range optical links," To appear in *IEEE Journal of Lightwave Technology*.

[H] K. Szczerba, P. Westbergh, M. Karlsson, P. A. Andrekson, and A. Larsson, "60 Gbits error-free 4-PAM operation with 850 nm VCSEL," *Electronics Letters*, vol. 49, no. 15, pp. 953–955, Jul. 2013.

[I] K. Szczerba, M. Karlsson, P. A. Andrekson, A. Larsson, and E. Agrell "35.2 Gbps 8-PAM transmission over 100 m of MMF using an 850 nm VCSEL," in Proceedings of the *39th European Conference on Optical Communication*, London, United Kingdom, Sept. 2013, paper Th.1.F.1.

Publications by the author not included in this thesis:

[J] J. S. Gustavsson, P. Westbergh, K. Szczerba, Å. Haglund, A. Larsson, M. Karlsson, P. Andrekson, F. Hopfer, G. Fiol, D. Bimberg, B.-E. Olsson, A. Kristiansson, S. Healy, E. O'Reilly and A. Joel, "High-speed 850-nm VCSELs for 40-Gb/s transmission," *Proceedings of SPIE*, vol. 7720, pp. 772002–7, Apr. 2010.

[K] J. Karout, K. Szczerba, E. Agrell, "Modulation scheme [Patent Application]," US Patent App. 12/976,188, Sept. 2010.

[L] K. Szczerba, P. Westbergh, J. Karout, J. S. Gustavsson, Å. Haglund, M. Karlsson, P. A. Andrekson, E. Agrell, and A. Larsson, "30 Gbps 4-PAM transmission over 200 m of MMF using an 850 nm VCSEL," in Proceedings of the *37th European Conference on Optical Communications*, Geneva, Switzerland, Sept. 2011, paper Tu.3.C.4.

[M] J. Karout, E. Agrell, K. Szczerba, and M. Karlsson, "Designing power-efficient modulation formats for noncoherent optical systems," in Proceedings of the *IEEE Global Communications Conference*, Houston, United States, Dec. 2011.

[N] J. Karout, E. Agrell, K. Szczerba, and M. Karlsson, "Optimizing constellations for noncoherent optical communication systems," *IEEE Transactions on Communications*, vol. 58, no. 7, pp. 4645–4659, Jul. 2012.

[O] R. Safaisini, Szczerba K., E. Haglund, P. Westbergh, J. S. Gustavsson, A. Larsson, P. A. Andrekson, "20 Gbit/s error-free operation of 850 nm oxide-confined VCSELs beyond 1 km of multimode fibre," *Electronics Letters*, vol. 48, no. 19, pp. 1225–1227, Sept. 2012.

[P] R. Safaisini, Szczerba K., P. Westbergh, E. Haglund, B. Kögel, J. S. Gustavsson, M. Karlsson, P. A. Andrekson, A. Larsson, "High-speed 850 nm quasi-single-mode VCSELs for extended-reach optical interconnects," *IEEE/OSA Journal of Optical Communications and Networking*, vol. 5, no. 7, pp. 686–695, Jul. 2013.

Acknowledgment

List of Acronyms

AB-QAM	Adaptively Biased Qadrature Amplitude Modulation
AOC	Active Optical Cable
AWGN	Additive white Gaussian Noise
BER	Bit Error Rate
BPSK	Binary Phase-Shift Keying
CAP	Carrierless Amplitude and Phase
DAC	Digital to Analog Converter
DC	Direct Current
DMD	Differential Mode Delay
DMT	Discrete Multi-Tone
EDFA	Erbium Doped Fiber Amplifier
EMB	Effective Modal Bandwidth
FEC	Forward Error Correction
HF	High Frequency
IM/DD	Intensity Modulation/Direct Detection
I/Q	In-phase and Quadrature
LED	Light Emitting Diode
MMF	Multi-Mode Fiber
MZM	Mach-Zehnder Modulator
OFDM	Orthogonal Frequency Division Multiplexing
OFL	Over-Filled Launch
OOK	On-Off Keying
OOPSK	On-Off Phase-Shift Keying
PAM	Pulse Amplitude Modulation
PAPR	Peak-to-Average Power Ratio
PSK	Phase-Shift Keying
QAM	Quadrature Amplitude Modulation
RF	Radio Frequency
RIN	Relative Intensity Noise

RS	Reed-Solomon
SFDR	Spurious Free Dynamic Range
SMF	Single-Mode Fiber
SNR	Signal to Noise Ratio
TIA	Transimpedance Amplifier
VCSEL	Vertical Cavity Surface Emitting Laser
WDM	Wavelength Division Multiplexing

Contents

1 Introduction

It is very often said that we are living in the information age. At the time of writing of this thesis around 77% of the population in the developed part of the world and 39% of global human population are connected to the Internet [1]. This percentage has been steadily increasing, as shown in Fig. 1.1. It has been enabled by new technologies which enabled processing, storage and transmission of information. Those technologies had and continue to have a very large impact on our societies and economies. We can affordably and quickly communicate with our business partners, family and friends around the planet. We can communicate not only using voice, we can also send large documents, images or videos. The economic impact of this is difficult to overestimate. Instead of going to a shop, we can purchase goods online and instead of renting a film we can use many of the available streaming services. A whole industry of business process outsourcing was enabled by low cost telecommunication services. Optical telecommunication systems play a significant, yet rarely visible role in delivering our information transmission needs. Fiber-optic communication systems form the backbone of mobile networks, where only the last link between the base station and the user is realized by radio transmission. The city, country and world spanning telecommunication networks are also based on the unique ability of guided light to transfer large amounts of data. Even the short-range networks in the data centers, which store online videos, our e-mails and other data, are dependent on optical communications. It is also those short-range optical links, which are the main focus of this thesis.
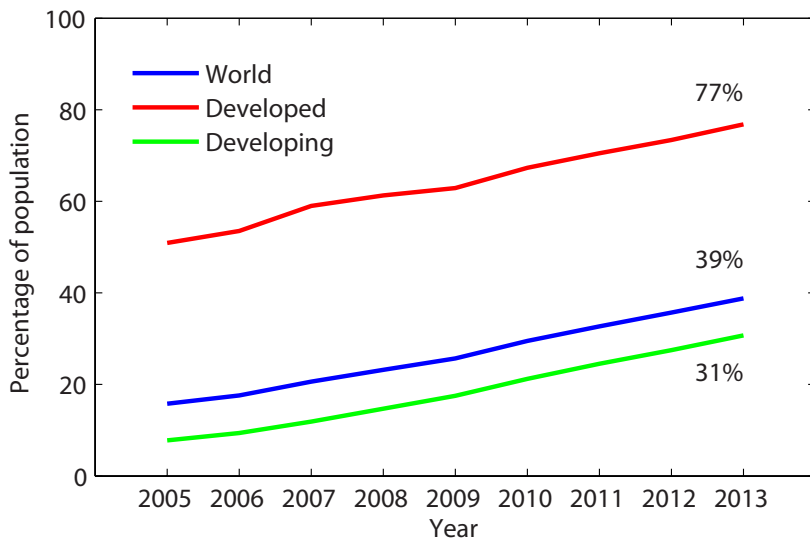
Figure 1.1: Percentage of population with Internet access, after [1].

1.1 History of optical communications

Optical communications is perhaps the earliest form of telecommunications to be employed, since smoke signals, semaphore lines and heliographs have been used for centuries. The development of electrical engineering in the nineteenth and twentieth century resulted in various forms of telecommunications based on copper wires. The technology has progressed from simple telegraph wires, through twisted pair cables to coaxial cables. Copper cabling is convenient, easy to use, and requires minimal training to manufacture, install and operate, but it has some shortcomings. It is heavy, and very lossy at high frequencies. Designs that minimize losses at high frequencies are very expensive. The development of an optical fiber in the 1960s [2] and early 1970s [3] came as a true breakthrough in the world of telecommunications. The simultaneous development of the semiconductor laser [4–7] has enabled the development of telecommunication systems as we know today. Due to the low cost and extremely low loss optical fibers became a mainstay of long-haul optical communications, but even with the low losses the signal eventually loses its power. In the early days of fiber-optic communications optoelectronic repeaters, which detected the signal

and re-transmitted it at higher power, were used. The disadvantage of this solution was that it made wavelength division multiplexing (WDM) very expensive. The development of Erbium doped fiber amplifiers (EDFAs) [8–10] in the late eighties enabled practical low cost WDM systems. Now, multiple wavelength channels could be amplified at once in a single device. The most recent step, which has managed to make its way from research labs to commercial products, was multi-level modulation and coherent detection. Coherent detection systems were investigated already before the rise of WDM systesm [11–13], but commercial coherent products (e.g. [14]) appeared only recently.

Today optical communications finds its place not only in long range transoceanic and transcontinental links, but it is advancing into other market niches, such as access networks which serve end customers, local and storage area networks which span server farms and supercomputers, down to the inside of the computers and networking equipment.

1.2   Short-range optical communications

In the area of short-range interconnect, Copper cabling has remained competitive until relatively recently, but today the industry is moving towards optical interconnects. The main markets for such interconnects are data centers and high performance computing. The demand for fast, reliable, power efficient, and low-cost interconnects has driven the development and market adoption of vertical cavity surface emitting lasers (VCSEL) [16]. With low-cost lasers available, the short-range optical links have already proliferated in the data centers, high performance computing, local area networks (LANs) and storage area networks [15], effectively dominating the market. Optical interconnects using VCSELs are also discussed for backplane interconnects inside computes [17–20]. Silicon photonics is a potentially competing technology in this application [21, 22].

Short-range optical links make their strides into new markets outside data centers, into applications such as consumer electronics and vehicular networks. Intel's new interconnect technology marketed under the name Thunderbolt, which was developed from an optical technology codenamed Light Peak includes active optical cables (AOCs) [23], which are optical fiber cables with integrated optoelectronic transceivers at the ends. The same will probably follow for the next USB standard [15]. The market for AOCs is already growing, because in addition to having advantages over
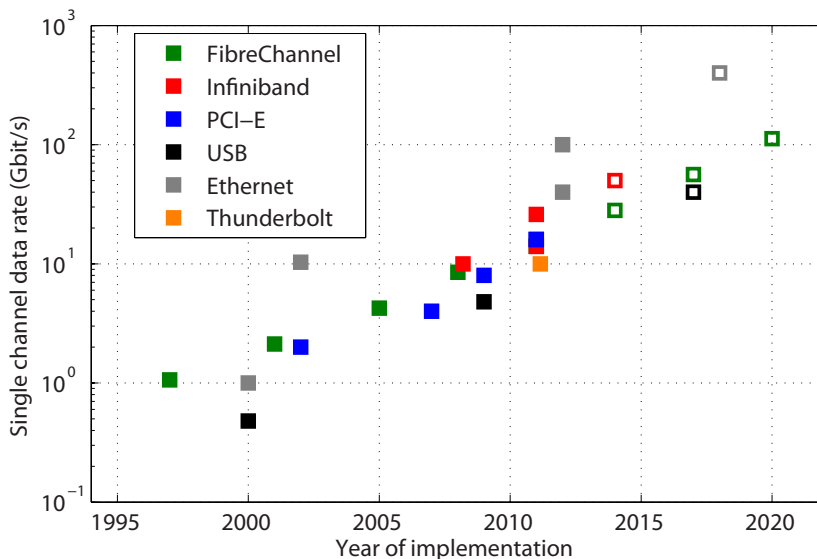
Figure 1.2: Interconnection throughput versus year of implementation. Open symbols indicate predictions [15].

copper cabling, such as lower weight, loss, cost, and increased transmission distance, they are easier to use for the end user. In case of AOCs the user deals only with electrical connectors at both ends. This has numerous advantages, for example, only the electrical interfaces are standardized, so the optical power budgets and modulation formats used can be designed according to the actual needs. Moreover, since the entire cable is sealed, eye safety, optical connector repeatability, loss and cleaning are avoided. The lack of optical connectors in AOCs can drive down the cost of such an optical interconnect and potentially give room for power budget for more advanced modulation. The low weight of optical fibers makes them interesting in vehicular networks. An example of optical networking technology for automotive applications is Media Oriented Systems Transport network, which has been in use for a few years now. Avionic optical networks are also investigated due to their light weight and robustness to electromagnetic interference [24–26].

To answer the market demand, the speed of optical interconnects has been steadily increasing, as show in Fig. 1.2. So far, the improvement has been largely due to continued development of faster VCSELs and detectors.

On the other hand, the throughputs and transmission distances of single fiber in short-range networks are already limited by the low bandwidth distance product of multi-mode fibers (MMFs), which are commonly used in such applications. Replacement of the MMF with single mode fiber (SMF) could be a possible solution, but that would require single mode lasers, more precise packaging and connectors which would drive the cost up. A more practical solution is to use parallel optical links utilizing arrays of transmitters and receivers, along with ribbon cables, in which many MMFs are bundled together, as it is stated in the new 40G/100G Ethernet standard [27]. The potential of such spatial multiplexing is however limited by the amount of space available in the transceiver, which is typically desired to be comparable in size to present small form-factor pluggable transceivers. Therefore, there is a need for an increased throughput and distance achievable with a single fiber in the short-range optical networking applications. It is possible is to minimize the differential mode delay (DMD) in MMFs [28] and to use single mode, narrow spectral width VCSELs, as demonstrated in [29, 30]. Another possibility is to apply more advanced modulation formats, which can achieve higher bit rates while maintaining low signaling rates, which will help to cope with the limited bandwidth-distance product of MMFs. Even with the development of improved types of MMF and parallel interconnects, advanced modulation formats will be relevant if they can provide increased bit rates or reaches at reasonable cost.

1.3   Objective of this work

The objective of this work is to investigate and develop advanced modulation formats for short-range optical communications. Because of the cost constraints, the considerations are limited to intensity modulation and direct detection (IM/DD) with directly modulated lasers. In IM/DD only the light intensity is detected which means that that the in-phase and quadrature components of the optical field cannot be accessed separately. The advantages are simplicity, small size and low power consumption as compared to differential or coherent detection, where interferometers and local oscillator lasers (in the latter) have to be used. Use of directly driven lasers means that costly and bulky Mach-Zehnder modulators (MZMs) are avoided. Directly modulated lasers do not require powerful driving amplifiers (as do MZMs) which translates to reduced system power consumption.

Although IM/DD excludes a wide range of coherent modulation tech-

niques, there are still many interesting modulation formats to investigate and plenty of possibilities to come up with new modulation formats. Some examples of known modulation formats of interest are pulse amplitude modulation (PAM) and subcarrier modulation. The simplest technique is PAM, which is an extension of on-off keying (OOK) into a multilevel format, where instead of two optical power levels any number M of power levels are implemented, where M is preferably a power of 2 for easy mapping of the symbols to bits. The subcarrier family of modulation formats leverages the experience from wireless data transmission and radio frequency (RF) photonics. A microwave subcarrier is first modulated using a modulation format such as e.g. phase-shift keying (PSK) or quadrature amplitude modulation (QAM) and later used to drive the VCSEL. The number of microwave subcarriers can vary depending on particular needs and constraints.

Apart from the PAM and subcarrier modulation a new family of modulation formats has been investigated. It combines the signal spaces of PAM and single subcarrier modulation into a three-dimensional signal space. It has been shown that modulation formats optimized in this signal space can have much better sensitivity than both PAM and single subcarrier modulation [31]. In this thesis results of experiments with all three families of modulation formats are presented.

1.4 Outline of the thesis

The structure of this thesis is a follows. The second chapter describes in general the short-range optical links, the components which are typically used, as well as noise sources and impairments present in this type of optical links. The third chapter is devoted to modulation formats which were investigated and developed. This chapter will cover mostly the experimental work. In the fourth chapter future work and prospects of the work done so far are given. The fifth chapter summarizes the published research contributions.

2 Short-range fiber-optic communication systems

2.1 Overview

In general, any communication system needs three basic components - a transmitter, a communication channel and a receiver. The transmitter takes the incoming digital data and converts it into a signal which can be transmitted over the communication channel. The communication channel is a physical medium used to transport the signal. Any physical channel has a limited bandwidth, adds noise to the signal, and causes other impairments, e.g. due to non-linearities of the components. The task of the receiver is to recover the original data sent by the transmitter as accurately as possible. The two fundamental properties, which characterize any communications channel, are bandwidth and signal-to-noise ratio (SNR) in the receiver. In 1948 Claude Shannon has shown that the channel capacity C is the following function of a channel bandwidth B and the SNR [32],

$$C = B \log_2(1 + \text{SNR}). \qquad (2.1)$$

It must be noted here, that this expression is valid only for linear channels with additive white Gaussian noise (AWGN). The channel capacity is the tightest upper bound on the amount of information, in bits per second, which can be transmitted over a given channel with arbitrarily small error probability. It does not tell us how to reach the highest possible bit rate, i.e. which modulation formats, or which coding schemes we should use. The described generalized communication system has to be implemented in some specific hardware. Typical short-range optical links have very strict
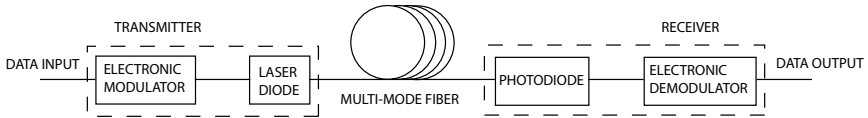
Figure 2.1: Model of a short-range communication system.

requirements which dictate the choice of hardware components. The interconnects in data centers have to be fast, power efficient and produce as little waste heat as possible. Because the number of interconnects is large, they must be small and low-cost. The most logical choice in such situation is to use low-cost directly modulated lasers, such as VCSELs, MMF and photodiodes for direct detection. The VCSELs are low-cost devices and they can be also designed for high speed operation. The state of the art VCSEL modulation bandwidths is 28 GHz [33] at the time of writing if this thesis. While the MMFs are more expensive per meter than SMFs, they have relaxed mechanical alignment tolerances and reduced overall cost. Because the amount of transceivers is very large, the packaging and connectorization is a major cost driver. The downside of using MMF and multi-mode lasers is that the reach of such system becomes very quickly limited by the modal dispersion, typically to 200 m for 10 Gbps in single MMF. Development of high speed single mode VCSELs compatible with today's MMFs promises reaches of above 1 km at 20 Gbit OOK operation, but the lasers need further development to meet the industrial requirements on reliability in a hot data center environment and ease of manufacturing. The receiver is subject to the same constraints as the rest of the system. For this reason, only simple photodetectors are used. Coherent receivers have better sensitivity, but the complexity, power consumption and cost are beyond the limits of short-range interconnects.

In such low-cost communication systems only IM/DD is possible. In contemporary systems on-off keying modulation is commonly used, as it is a simple modulation format and requires a minimum of electronic processing. Moreover, it relaxes requirements on linearity of the components and enables use of limiting amplifies, which help maintaining the signal integrity throughout the system. Modulation formats which would be applied in such optical links would also have to balance performance with the complexity of the electronics. On the other hand, with short-range optical links expanding into other applications, it is possible that the trade-offs

will be different, and more complex modulation formats could be accepted. For example, today's Gigabit Ethernet over CAT5 cabling made of parallel twisted pair lines uses coded multilevel modulation, using each twisted pair as an additional modulation dimension [34, Section 1]. At data rates of 1Gbps, this is still a low cost solution. A general model of a short-range optical communication system is presented in Fig. 2.1. The optoelectronic part of the system comprises a directly modulated laser diode, MMF and a photodetector. The electrical signal driving the laser is provided by an electronic modulator and the optical signal detected by the photodetector is handled by an electronic demodulator.

A detailed description of the directly modulated laser, MMF and signal detection is provided in Sec. 2.2–2.4. Modulation is the topic of Chapter 3.

2.2   Directly modulated lasers

The optical part of the link begins with the directly modulated semiconductor laser. Such lasers are power efficient and reliable [35, Ch. 1], with overall power conversion efficiencies around 50 % not being uncommon. The word "laser", although a noun in its own right today, originates from an acronym for *Light Amplification by Stimulated Emission of Radiation*, which shortly summarizes how lasers work. There are two basic components of any laser – an optical resonance cavity and an optical gain medium, which in our case of interest is a semiconductor material. A photon travelling through the gain medium is able to generate an identical photon through stimulated emission, i.e. stimulating the recombination of an electron-hole pair. The emitted photon has the same wavelength and phase (i.e. the same quantum state) as the stimulating photon. The resonance cavity provides a means of confinement of the photons, which leads to subsequent repetition of the light amplification process. The optical resonance cavity is usually formed between two mirrors, which can be built in many different ways. To enable resonance, the cavity round-trip distance must be an integer number of wavelengths. The resonance can happen only for a discrete number of wavelengths and the separation between them is inversely proportional to the cavity length.

The gain medium in an electrically pumped semiconductor laser usually consists of an intrinsic (undoped) layer of a semiconductor material, placed between p- and n- doped layers. This forms a semiconductor diode. When the diode is forward biased, charge carriers (electrons and holes) ac-

cumulate in the intrinsic layer. Electrons in the conduction band states can transit to lower energy states in the valence band, emitting the surplus energy as light. The transitions can be either spontaneous or stimulated. The bandgap of the semiconductor material used must correspond to the energy of photons at desired operation wavelength. As the current is increased, the number of carriers available for stimulated emission is increased, and consequently the gain. When the gain exceeds the loss, which is due to absorption and mirror losses, the lasing threshold is reached. The current at which this happens is called the threshold current. For most applications a low threshold current is desired.

There are many varieties of semiconductor lasers, starting with multiple possibilities of forming resonance cavities in semiconductor lasers – from simple Fabry-Perot type of cavities formed by cleaving of the edges of the laser chip through distributed feedback reflectors (DFB) to external mirrors for tunable lasers. The choice of material for the laser is largely dictated by the required operation wavelength. For optical interconnects the wavelength of operation is standardized at around 850 nm [27] and therefore GaAs-based materials are used. Light emitting diodes (LEDs) were used in legacy short-range communication systems, but they do not have sufficient modulation bandwidth for modern applications.

In short-range optical links the laser combines the functions of light source and modulator. In long reach systems directly modulated lasers are usually avoided, because of large chirp, which increases the severity of chromatic dispersion. This is not a major concern in short-range links. A directly modulated VCSEL eliminates the bulky external modulators which often require high driving voltages and so it became the preferred transmitter. The sections 2.2.1-2.2.6 are devoted to VCSELs, focusing on their properties and behaviour.

2.2.1 Vertical Cavity Surface Emitting Lasers

VCSELs were proposed nearly three decades ago by the Japanese scientist Kenichi Iga [36], although there were early forerunners already in the 60's [37]. They gained significant popularity during the last decade [16]. This type of laser emits radiation from the surface, in a direction perpendicular to the substrate. The main benefit of this is that the lasers can be easily tested on the wafer, before dicing or packaging, which greatly reduces the production costs. The resonant cavity is most commonly formed by reflectors comprised of alternating layers of high and low refractive index
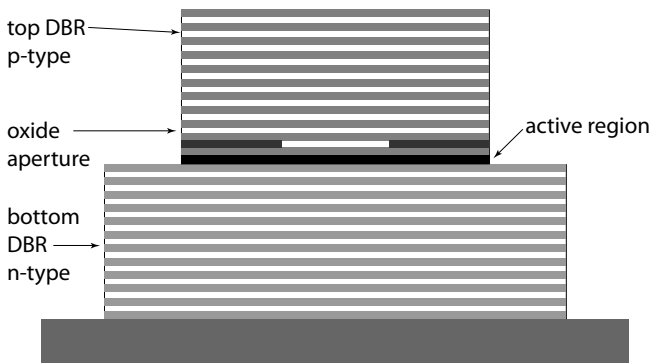
Figure 2.2: Example of a modern VCSEL structure designed for communications applications.

material, parallel to the substrate, forming high quality distributed Bragg reflectors (DBRs). At least one of the reflectors must be partially transmissive to enable extraction of light from the laser. The resonance cavity is located between the reflectors. Lateral confinement can be provided by various means. In modern GaAs-based high-speed VCSEL designs it typically done with oxide apertures. The resonance cavity is perpendicular to the substrate and is very short and wide. This geometry supports a single longitudinal and multiple transverse optical modes. Light is emitted from the laser vertically, along the direction of the cavity. In the resonance cavity, there is a gain region formed by a *pin* junction. An example of a modern VCSEL structure is illustrated in Fig. 2.2. Detailed description of VCSEL design, fabrication and operation can be found today in numerous handbooks [38–41]. The popularity of VCSELs can be attributed to some of their unique properties, like longitudinal single mode operation, large modulation bandwidth and high quality circular beams. The most important features are, however, low-cost fabrication and low power consumption [42]. Current state of the art (i.e. lowest) energy dissipation in a VCSEL used for data communication is below 100 fJ per bit at 25 Gbps [43, 44].

2.2.2 Static characteristics

The basic static property of any semiconductor laser is how the optical output power P depends on the electrical current I driving the device. An example plot of a VCSEL optical output power as a function of driving cur-
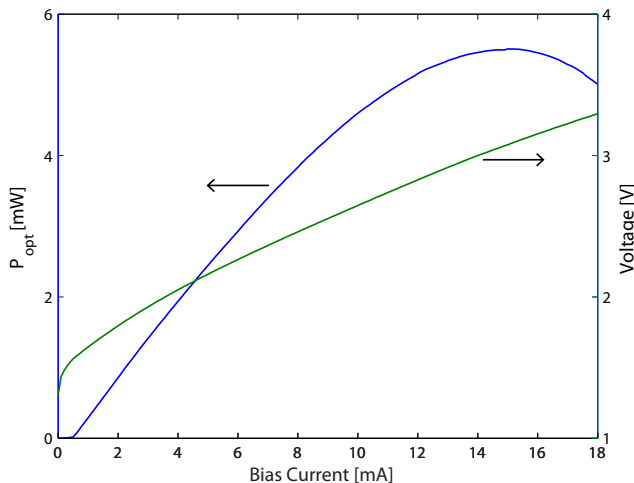
Figure 2.3: Optical output power and voltage as a function of current for a VCSEL.

rent is illustrated in Fig. 2.3. The plot includes also voltage V across the device as a function of current. Looking closely at Fig. 2.3 one can notice that the optical output power is very small for currents below the threshold current, which is around 0.5 mA. The output power rapidly increases above the threshold current. The growth is linear at low currents, but it saturates at some point and begins to decrease with increased current. This happens due to thermal effects, since the increased current contributes to increased heating inside the device.

Knowledge of the relation of the optical output power and voltage across the device as a function of the bias current gives also insight into the laser power efficiency, which is given by $\eta = P/(IV)$, where P is the optical output power, I is the current and V is the voltage across the laser. Obviously, the higher the efficiency the better, since less energy is wasted as heat.

The high speed VCSELs used for datacommunications are usually low-power devices, with maximum output powers rarely exceeding 10 mW. The threshold currents are very low and the operation is quite efficient, which is important from a power consumption point of view.

2.2.3 Linearity

The usable dynamic range of any real life device is limited, and the same holds for VCSELs. One has to keep in mind that the static characteristics of any laser is relevant for static operation only and offers only a limited insight into dynamic properties. The dynamic non-linearities are better described by the spurious free dynamic range (SFDR) [45]. Non-linearities in lasers give rise to harmonics and intermodulation products. If the modulation depth is small, the distortions are below the noise floor, but as the modulation depth increases, the distortions rise above the noise floor. The dynamic performance, relevant e.g. for data transmission is usually much better than the static measurements would suggest, because the modulation frequencies are typically much higher than the bandwidth of the thermal response [46]. In general the SFDR increases with the bias current, and may continue to increase beyond the thermal roll-over point of the static optical output power vs. current characteristics [47]. The linearity of the laser is important, because it affects and distorts the modulation that is imposed upon the device. The non-linearity does not have great influence on simple modulation formats, such a OOK, but becomes more important for multilevel modulation formats. While exact quantification of penalties due to the non-linearity is quite complex, in general modulation formats with high peak-to-average power ratio (PAPR) require higher linearity.

2.2.4 Spectral characteristics of VCSELs

Most of the VCSELs available today have a single longitudinal mode and multiple transverse modes. As each of the transverse modes has a slightly different wavelength, this results in a rather broad spectrum of the laser. An example spectrum of a multi-mode VCSEL is presented in Fig. 2.4. To make matters more complicated, the number of lasing modes changes with the bias current, with more modes at higher bias currents. It also worth noticing, that the laser spectrum is much broader than the bandwidth of the modulating signal. For example, a spectral width of 1 nm at 850 nm corresponds to a bandwidth of 415 GHz, which is much higher than the typical modulation bandwidth. Therefore, the spectral efficiency of the modulation becomes irrelevant, since effects related to e.g. chromatic dispersion will be dominated by the spectral width of the laser itself. It was shown that VCSELs with fewer transverse modes and narrower spectral widths can enable longer transmission distances in MMF [29, 30, 48]. Therefore,
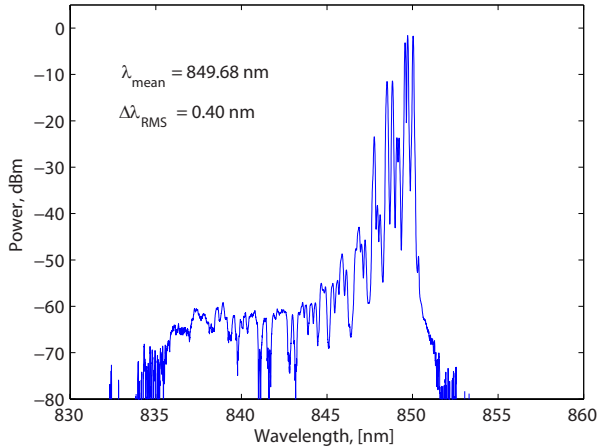
Figure 2.4: Example of a spectrum of a multi-mode VCSEL.

many standards dealing with short-range optical communications have recommendations on the root mean square (RMS) spectral width of the lasers used in the transmitters. For example, Ethernet specifies 0.6 nm as the maximum spectral width for 10 Gbps lanes [34, Sec. 6].

It is possible, however to make single mode VCSELs, with very narrow spectral widths. Transmitters with narrower spectral widths, such a single mode VCSELs, can yield higher bandwidth-distance products. Single mode VCSELs can be made for example by using smaller oxide apertures e.g. as the ones used in [29, 30], or increasing the loss for higher order modes [48]. The result is a laser with narrower spectral width. This improves propagation in MMF and helps reach longer distances at high bit rates, while still retaining the ease of connectorization of MMF.

2.2.5 Frequency response

The frequency response of a VCSEL is one of the key parameters from the point of view of the system design. In general, the frequency response of a semiconductor laser is flat at low frequencies, possibly with a peak at the resonance frequency, and then it has a fast roll-off [35, Ch. 2.7]. The frequency response depends not only on the laser design, but also on the bias current. The larger the bias current, the higher the resonance frequency. This relationship holds until thermal saturation effects take over,

Figure 2.5: Frequency response of a VCSELs for bias currents in range 1 mA to 5 mA.

Figure 2.6: A setup used to measure the frequency response. For back-to-back measurements only a short fiber patchcord is used.

in effect limiting the maximum bandwidth. The presence of a strong resonance peak also has a significant effect on data transmission, as it causes an overshoot on symbol transitions, and this can be detrimental for multilevel data transmissio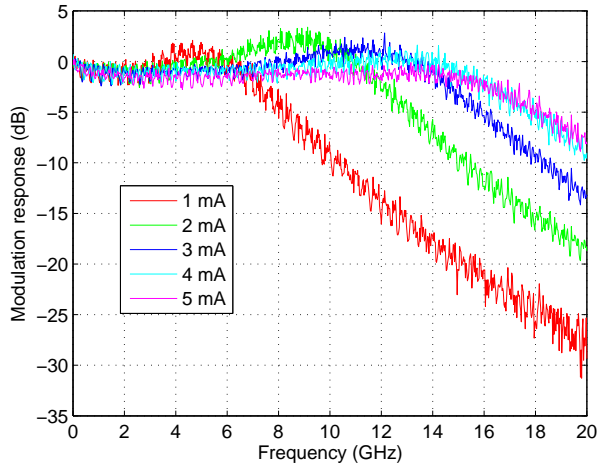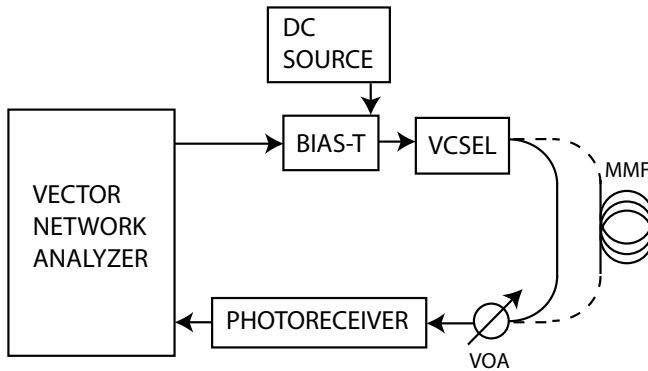n. An example of a frequency response of a VCSEL used in the experiments described in this thesis is illustrated in Fig. 2.5. The frequency response was measured in a back-to-back configuration, with a short MMF patchcord and a sufficiently fast photodetector.

The current state-of-the-art VCSEL modulation bandwidth is around 28 GHz, reported in [33]. With this VCSEL data rates up to 47 Gbps were achieved with a limiting photoreceiver [33] and up to 57 Gbps with a linear photoreceiver [49]. The same laser was used for 60 Gbps 4-PAM demonstration presented in Paper H. In [50] 56.1 Gbps was demonstrated with use of specially designed drivers and equalizer circuits. Other previously reported results using OOK were at data rates around 40 Gbps [51, 52], although the modulation bandwidth of the devices were not stated, such data rates imply that the modulation bandwidth exceeds 20 GHz.

Currently 10 Gbps is the industry standard, and for higher data rates multiple parallel 10 Gbps links are often aggregated, such as in case of 40G/100G Ethernet [27], because transmission distance in MMF with OOK at higher data rates becomes limited. There is an ongoing effort to increase the single-lane bit rates. Fibre Channel has included in the standard single-lane speeds up to 14 Gbps [53, 54] and QSFP modules with four parallel 25.78 Gbps lanes have been demonstrated [55].

2.2.6 Laser noise

Relative intensity noise (RIN) is caused by the coupling of the spontaneous emission into the lasing modes. This causes unwanted fluctuations of the optical power, thereby generating a noise current in the optical receiver circuit, which translates to an optical power penalty in the data link. RIN is measured into a finite bandwidth optical system, and is thus quoted in terms of dB/Hz.

Another source of optical power noise is the feedback of stray optical reflections into the laser. This is an unavoidable effect common to all laser systems, and proper engineering of the optical assembly is required to minimize its effects. The optical power in a multi-mode VCSEL is partitioned between several lasing modes, so modal noise can occur when one of the modes is discriminated. Polarization-selective elements, such as beamsplitters and some couplers, can also produce this kind of noise [56]. To

minimize such effects as many VCSEL lasing modes as possible should be coupled into the fiber in order to prevent mode partition noise.

2.3 Multi-mode fibers

The MMF is the most popular type of optical fiber in short-range optical interconnects today. The main advantage of the MMF is a large core area, which relaxes alignment tolerances in coupling, makes launching light from the transmitter easier and reduces costs. This was very important in legacy systems using LED sources. The disadvantages of MMF, compared to e.g. SMF are higher cost per meter and intermodal dispersion. The higher cost per meter is offset by the fact that in a data center with a large number of short links the connectorization is a bigger cost-driving factor. The intermodal dispersion causes pulse broadening at the end of the fiber and reduces the bandwidth-distance product.

2.3.1 Multi-mode propagation

The typical MMF core diameter is between 50 μm and 62.5 μm. For comparison, a typical SMF has a core diameter of 9 μm. The light guiding mechanism in an MMF is the same as any other dielectric waveguide, a core of refractive index n_0 is surrounded by a cladding with a refractive index $n_1 < n_0$. Due to total internal reflection, the propagating light is trapped inside the core, as long as the incidence angle at the core-cladding interface is smaller than the critical angle (defined with respect to the fiber axis). This simple description does not, however cover the entire picture. The field of the propagating wave has to repeat itself as it reflects at the interface. The fields that satisfy this condition are called modes of the waveguide [57, Ch. 7]. The fields of the modes maintain the same transverse distribution and polarization along the waveguide. From a mathematical point of view, modes are a solution to the electromagnetic wave equation in the waveguide, in this case, an MMF. The wave equation for weakly guiding dielectric waveguide, where $n_1 - n_0 \ll 1$ can be simplified to a scalar wave equation [58, Ch. 14]

$$(\nabla_t^2 + k_0^2 n^2(r) - \beta^2)E_t(r,\theta) = 0, \tag{2.2}$$

where E_t give the transversal electric field profile defined in the cylindrical coordinate system normal to the fiber axis given by (r,θ), k_0 is the wavenumber, β is the propagation constant and $n(r)$ gives the refractive
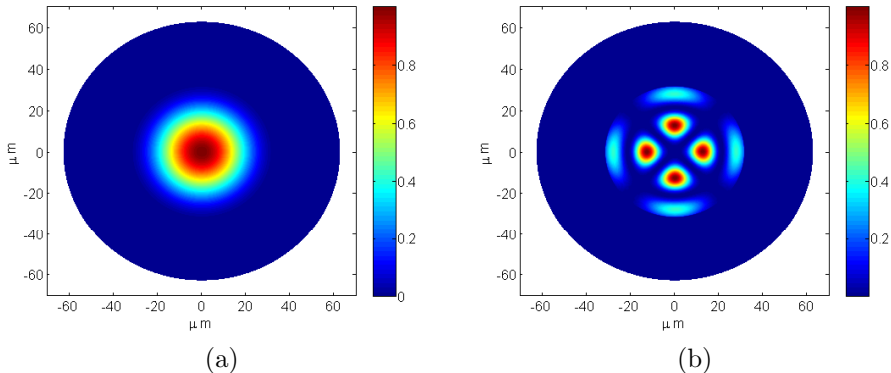
Figure 2.7: Intensity profiles for LP_{01} and LP_{22} modes in a step index fiber with 62.5 μmcore diameter and 1% refractive index contrast between the core and the cladding.

index profile, which is assumed to be axially symmetric around the fiber axis. The solutions to this equation are the linearly polarized modes, commonly denoted as LP_{jk} modes, with subscript indexing for the radial and azimuthal orders of the mode, respectively. As an example intensity profiles for LP_{01} and LP_{22} modes in a step index fiber with 62.5 μmcore diameter and 1% refractive index contrast between the core and the cladding are shown in Fig. 2.7. The LP_{01} is the fundamental mode, and in SMFs it is the only mode of the fiber. The number of modes in a fiber can be calculated using the V parameter [57, Ch. 8],

$$V = 2\pi \frac{a}{\lambda} \sqrt{n_1^2 - n_0^2}, \tag{2.3}$$

where λ is the wavelength of the light propagating in the fiber and a is the core diameter. For fibers with large V the number of modes can be approximated as

$$N_{modes} \approx \frac{4}{\pi^2} V^2, \tag{2.4}$$

as given in [57, Ch. 8]. For fiber with a core diameter in the range between 50 μm and 62.5 μm, with a core refractive index of 1.5, and 1% index contrast between the core and the cladding, the number of supported modes is between 600 and 900. An arbitrary transverse electric field in a dielectric waveguide can be written as a superposition of guided modes possible for

18

a given waveguide [57, Ch. 7],

$$E(x, y, z) = \sum_{j,k} a_{j,k} u_{j,k}(x, y) \exp(-j\beta_{j,k} z), \qquad (2.5)$$

where for each mode m, a_m is the mode amplitude, $u_{j,k}(x, y)$ is the mode distribution and β_m is the propagation constant of each mode. The propagation constant is different for each mode, and since the group velocity v_g is dependent on the propagation constant β as

$$\frac{1}{v_{g,j,k}} = \frac{\delta \beta_{j,k}}{\delta \omega}, \qquad (2.6)$$

where the ω is the angular frequency. The group velocity of each mode may be different. This translates to a differential mode delay between modes[59], and in effect causes the modal dispersion. Different launch conditions can excite different groups of modes, giving rise to unpredictable performance of the MMFs, particularly when older types of fiber designed for overfilled launch (i.e. exciting all modes) with LEDs are used with laser transmitters [60]. On the other hand, it has been demonstrated that under special coupling conditions the propagation reach in MMF can be dramatically increased [61]. It would seem, that given the amount of modes, the modal dispersion will be too large to achieve any reasonable transmission distance in MMF. There are however mode groups with identical or similar group velocities, and they can be grouped together in principal mode groups. Modes LP_{jk} belong to the same principal mode group m if they fulfill the condition [62]

$$m = 2k + j - 1. \qquad (2.7)$$

The number of modes in a group increases with the group number m, with the lowest-order group containing on the fundamental mode [63]. Since the modes in a mode group have similar properties, they can be treated in terms of mode groups, rather than individual modes [64].

2.3.2 Graded-index fibers

Given that there are many mode groups in an MMF, each with different group velocity, it is important to design the fiber in such a way, that it minimizes the spread in propagation between different modes. This is achieved when the refractive index is highest at the fiber axis and gradually decreases
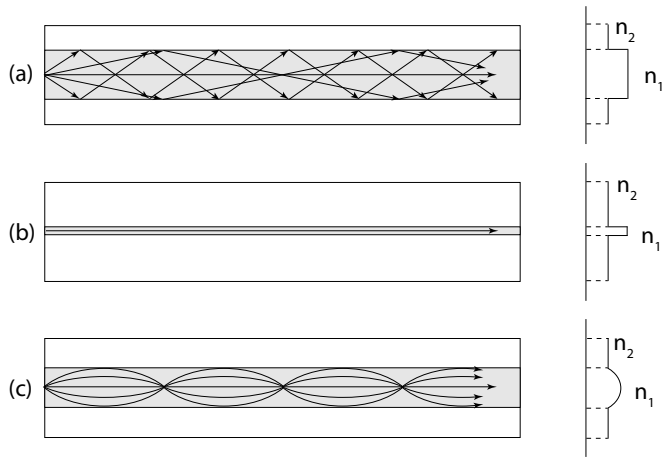
Figure 2.8: Ray optics approximation of light propagation in optical fibers – (a) step index MMF (b) SMF (c) graded-index MMF.

towards the cladding [65]. It is common for the cores of graded-index fibers to follow power-law index profile [64] given by [57, Ch. 8].

$$n^2(r) = n_a^2 \left[1 - 2 \left(\frac{r}{a} \right)^p \left(\frac{n_a^2 - n_1^2}{2n_a^2} \right) \right], \quad r \le a, \tag{2.8}$$

where n_a is the refractive index at the fiber axis, n_1 and p is the profile exponent. For an optimized value of the profile exponent, the differential mode delays can be nearly eliminated [62]. The optimal profile exponent is dependent on fiber material and the wavelength of light which is supposed to be used. Note that the index profile can be optimized at only one wavelength. Apart from intermodal dispersion there is also chromatic dispersion. Multi-mode VCSELs have sufficiently broad spectrum to suffer from this problem [28]. Single-mode VCSELs operating at 850 nm and with sufficient output power and low manufacturing cost [66] could help to avoid it. The launch conditions are also important, as the number of excited modes and power distribution between the modes is going to influence the impulse response of the fiber.

2.3.3 Ray optics description

As it was shown in the previous section, the full mathematical description of multiple mode propagation is rather complex. Therefore, for pedagogical
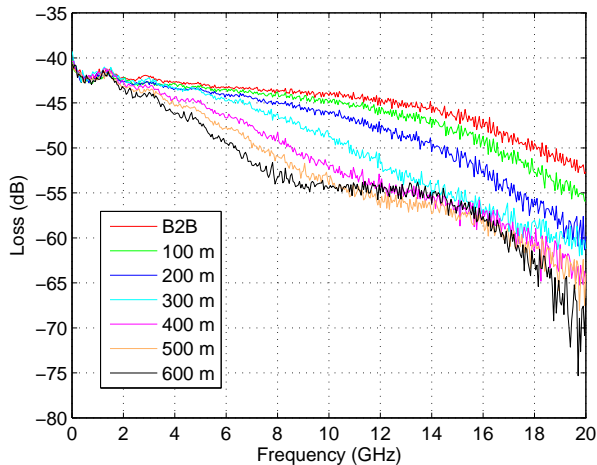
Figure 2.9: Frequency response of a fiber-optic link built with a VC-SEL and OM3+ MMF.

purposes the MMFs are very often illustrated using ray optics approximation. This model, valid for MMFs with large core diameters, is useful e.g. intuitive understanding of differences between step index MMFs and graded-index fibers. The ray propagation of light propagation in step index MMF, SMF and graded index MMF is illustrated in Fig. 2.8. In a step-index MMF the rays at higher inclination from the fiber axis have travel a longer distance before they reach the end of the fiber. In an SMF there is only one ray corresponding to the single mode propagating in the fiber, which circumvent the entire problem of different propagation delays. In graded index fibres the refractive index is decreasing in the direction away from the core, so the rays of greater inclination travel faster, which to some extend compensates for their longer travel distance through the fiber [57, Ch. 8].

2.3.4 Impulse and frequency response

When the power distribution over the different modes and propagation delays of each mode are known, the impulse response of the fiber can be estimated. If the fraction of power in each of the LP_{jk} modes is denoted

21

$p_{j,k}$ the impulse response of an MMF of length L can be expressed as

$$h_{MMF} = \sum_{j,k} p_{j,k} \delta(t - \frac{L}{v_{g,j,k}}).$$
(2.9)

The frequency response can be readily obtained from the impulse response with a Fourier transform. The frequency response of the fiber is dependent on the source type and launch conditions into the fiber. For example LEDs usually excite all modes in the fiber and consequently for LED transmitters an *over-filled launch* (OFL) condition is used. The fiber bandwidth under OFL condition is usually given for fibers foreseen for use with LEDs. For fibers optimized for use with VCSELs the *effective modal bandwith* (EMB) is given [67, 68]. The EMB is calculated using (2.9) from the DMD which is measured by selectively exciting different mode groups. To measure the DMD a single mode fiber is used to launch short pulses at different radial offsets from the center. Usually, the entire range from the fiber axis to the cladding is scanned. Launching light into the MMF at lower radial offset excites lower order mode groups and launching at high radial offsets excites higher order mode groups.

The frequency response of the fiber can be conveniently measured by e.g. a vector network analyzer (VNA) using the same setup as for the VCSEL frequency response measurement. The setup is illustrated in Fig. 2.6. An example of frequency response measured for a link built with a VCSEL and OM3+ MMF, with various lengths of the fiber is illustrated in Fig. 2.9. The OM3+ fiber has a bandwidth-distance product of 4700 MHz $\cdot$ km, defined for laser launch, at the wavelength of 850 nm. As it can be seen in Fig. 2.9, the bandwidth of the link is decreasing with the increasing length of the fiber. The frequency response of older step index fibers experiences multiple lobes beyond the main passband and it has been proposed that multiple subcarrier modulation can be used to take advantage of those lobes for data transmission [69]. This is relevant mostly as an upgrade to existing systems using legacy MMF.

A promising way of increasing the transmission distance in modern MMF is to use single mode VCSELs operating at the wavelength for which the fiber was optimized. At this wavelength the optimized index profile guarantees very low DMD, and a narrow spectral width reduces the effects of chromatic dispersion [70]. This was shown to work in practice, transmission over 1 km of OM4 MMF with a single mode VCSEL was demonstrated in [29, 30]. On the other hand, long term reliability (i.e. lifetime) of single mode VCSELs is yet to be established [66, 71].

Table 2.1: Bandwidth-distance products of standardized types of MMF.

Fiber type	OFL bandwidth [MHz×km]	EMB [MHz×km]
OM1	200 at 850 nm 500 at 1300 nm	Not specified
OM2	500 at 850 nm 500 at 1300 nm	Not specified
OM3	1500 at 850 nm 500 at 1300 nm	2000 at 850 nm
OM4	3500 at 850 nm 500 at 1300 nm	4700 at 850 nm

2.3.5 Standardized types of MMF

There are three bodies that standardize the MMF commonly used in short-range data communications, the International Electrotechnical Comission (IEC) which works together with the International Standards Organization (ISO) and the Telecommunications Industry Association (TIA). At the time of writing of this report there are four main types of MMF standardized and intended for data communications, OM1, OM2, OM3 and OM4. The types OM1 to OM3 are defined in the standard ISO/IEC 11801 [72]. There OM4 type of fiber is defined in TIA-492-AAAD and ISO/IEC 60793-2-10 as fiber type A1a.3. The standards define the performance requirements for various types of fiber, but do not define the how the performance is to be achieved. There are only some constraints on geometry and numerical aperture to ensure proper coupling. The OM1 and OM2 types can have core diameters of 50 μm or 62.5 μm, with 125 μm cladding diameter. The OM3 and OM4 fibers are standardized at 50 μm. The definition of the numerical apertures, core and cladding geometry tolerance (such as non-circularity) of the OM1 to OM3 fiber in the standard ISO/IEC 11801 is referred to the standard IEC 60793-2-10. There was an interim OM3+ specification adopted in the industry in anticipation of the OM4 standard. The performance requirements for OM3+ are the same as for OM4. A summary of the performance requirements for the various fiber types is given in Table 2.1. All fiber types are required to have attenuation below 3.5 dB/km at 850 nm and below 1.5 dB/km at 1300 nm. The OM1 and
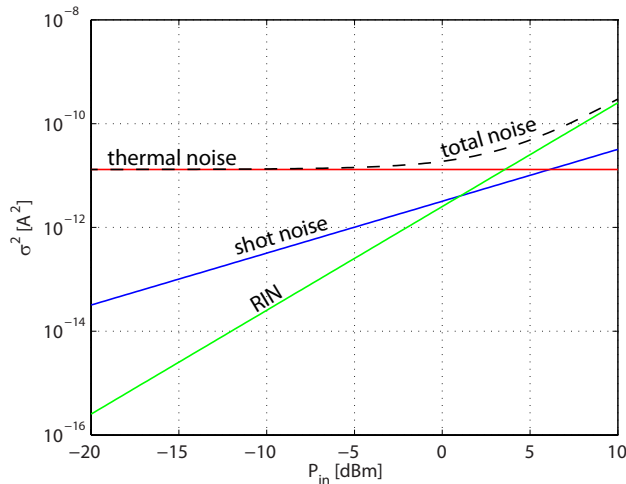
Figure 2.10: Contributions from the thermal noise, shot noise and relative intensity noise for given system parameters at receiver bandwidth of 12.5 GHz.

OM2 standard were defined back in the days when the main transmitter type used in low cost application was an LED, therefore only the OFL bandwidth is defined. The new fibers, OM3 and OM4, define both the OFL bandwidth for backwards compatibility, but the main relevant parameter is the EMB for laser launch.

2.4 Signal detection and noise

The task of an optical receiver is to convert the incident optical power P_{in} into an electric current. The most common device performing this task is a *pin* photodetector. The output current is directly proportional to the incident optical power, the relationship is given by $I = R_d P_{in}$, where the R_d is the responsivity of the photodiode. The photodiode is usually followed by an electrical amplifier, which then is followed by a decision circuit or a more sophisticated demodulator. Two types of amplifier configurations are possible – a transimpedance amplifier (TIA) and a voltage amplifier. A TIA has ideally zero input impedance, the input signal is a current and the output signal is voltage [73, Ch. 14]. The other type is a voltage amplifier, which has voltage input and voltage output. Since a photodiode can be re-

garded as a current source [73, Ch. 14], a TIA is a better amplifier choice.

The output of the photodiode contains also undesired noise. The performance of the system depends on the SNR, which is defined as follows

$$SNR = \frac{\text{average signal power}}{\text{noise power}} = \frac{\bar{I}^2}{\sigma^2}, \tag{2.10}$$

where $\bar{I}$ and σ are respectively, the average photocurrent and the root mean square noise current. It is important to note that the SNR is defined in the electrical domain and the noise is measured in the electrical domain after the detection of the optical signal. The performance of a system is given by the receiver sensitivity, which is the amount of optical power needed to operate below a specific bit error rate (BER). In direct detection systems, the electrical power is proportional to the square of the optical power (square law detection).

There are three noise sources which are relevant in IM/DD systems:

1. shot noise,

2. thermal noise,

3. relative intensity noise (RIN).

The shot noise originates from the quantum nature of light and current. Even if constant optical power is incident on the photodiode, the photon absorption and electron-hole generation processes happen at random time intervals. This gives rise to a random variation of the signal current. The variance of the shot noise is

$$\sigma_s^2 = 2qI\Delta f, \tag{2.11}$$

where q, I, and Δf are respectively the elementary charge, the photocurrent, and the receiver bandwidth [74, Sec. 5.1.1]. It is apparent, that the variance of the shot noise increases with the photocurrent (and thus with the average optical power).

The thermal noise comes from the fact that at any temperature above the absolute zero the electrons are moving inside the conductor and the thermal motion of the electrons manifests itself as current noise. The variance of the thermal noise is given by

$$\sigma_t^2 = 4k_BTF_n\Delta f/R_L, \tag{2.12}$$

where k_B, T, F_n, and R_L are respectively, the Boltzmann constant, the temperature, the noise figure of the amplifier following the photodiode and the load resistance [74, Sec. 5.1.2]. This noise contribution is not dependent on the signal power.

The RIN originates in the laser. The carrier generation and recombination process in a semiconductor laser is random in its nature and gives rise to noise. The RIN spectrum is not white, it peaks at resonance frequency, and for multi-mode lasers (such as those used in the discussed applications) also at low frequencies due to mode competition [75]. The noise variance of the RIN after the photodetector is

$$\sigma_{RIN}^2 = S_{RIN}I^2\Delta f, \qquad (2.13)$$

where S_{RIN} is the RIN value (often expressed in dB/Hz [74, Sec. 5.4.2]). It is worth noting, that the variance of the RIN is also dependent on the signal power, just as the shot noise, but in this case, the noise variance is proportional to the square of the photocurrent.

It is important to realize how much noise there is present and which noise sources dominate, as this determines the performance of the link and potentially also design of the modulation. The following parameters illustrate well the system used in the experiments presented in this work, $R = 0.4$ A/W, $T = 298$ K, $F_n = 5$ dB, $R_L = 50$ Ohm and $S_{RIN} = -155$ dB/Hz. To illustrate the relationship between the three noise contributions for the given parameters, they are plotted against received optical power P_{in} in Fig. 2.10. The RIN and shot noise are stronger than the thermal noise only for received power levels greater than 3 dBm. On the other hand, the photodetectors used in our experiments have saturation power levels at around 3 dBm received optical power, so it is apparent that the system is always dominated by the thermal noise.

2.5 Communications channel model

Although the physical description of the short-range communication system is interesting, it is useful to present a simplified mathematical model, which can be used for modulation format design. Such a model, presented also in [76], is illustrated in Fig. 2.11. The modulator maps the symbols $u(k)$, at an instant k to a waveform $x(t)$. The received signal is $y(t)$ and can be written as

$$y(t) = x(t) + n(t), \qquad (2.14)$$
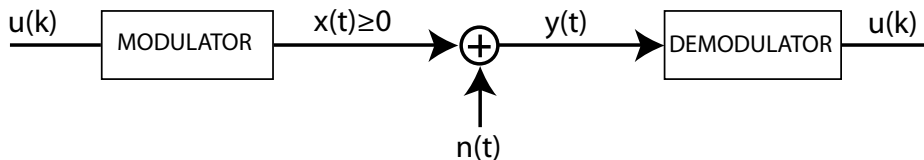
Figure 2.11: Communication system model.

where $n(t)$ is the added noise. The demodulator uses $y(t)$ to provide an estimate of $u(k)$, which is denoted $\hat{u}(k)$. There is a non-negativity constraint on the signal $x(t)$, since it is used to modulate the directly modulated laser. The laser operates only if it is forward biased, and thus the driving signal must be non-negative. From Sec. 2.4 it follows that the main noise source is the thermal noise. This type of noise can be characterized statistically as AWGN [77, Sec. 1.3] and therefore the considered system can be treated as an AWGN channel with non-negativity constraint. It should be noted that there is no non-negativity constraint on $y(t)$. This channel model has been analyzed in detail in the communications literature, e.g. [78, 79].

2.6 Standards in short-range optical communications

There are three competing standards for short-range optical communications:

- Ethernet,

- Fibre Channel,

- Infiniband.

Ethernet is the broadest of them, as it governs all kinds of local and metropolitan area networks, based on copper and fiber links, operating at bit rates from 10 Mbps to 100 Gbps. It was commercially introduced in 1980 and standardized by the Institute of Electrical and Electronics Engineers (IEEE) in 1985 as IEEE 802.3, which is a part of the IEEE 802 family of standards governing local and metropolitan area networks. The parts of the Ethernet standard which define the physical layer for short-range optical communication are described in Section 6 of the IEEE 802.3-2012 [34].

The standard is a subject to continuous work and new iterations are published every few years. The most recent version of the standard at the time of writing of this work was published in 2012 and foresees data rates up to 100 Gbps using ten parallel lines. Previously, the parts of the standard relevant for short-range optical links were maintained in a separate document, the IEEE 802.3ba [27], but all the sub-documents describing the Ethernet standard were superseded by the IEEE Std 802.3-2012 and are no longer maintained as separate documents. There are three speeds at which the optical Ethernet version can be used: 10 Gbps, 40 Gbps and 100 Gbps. For the short-range applications, up to 400 m use 850 nm lasers with MMF is foreseen, with maximum transmission distance being a function of the EMB [34, Sec. 4]. For the 10 Gbps case 7.5 dB optical power link budget is foreseen. The 40 Gbps and 100 Gbps links are created by parallel aggregation of four or ten 10 Gbit links, with the same wavelength and fiber types at the 10 Gbps Ethernet. The optical power link budget is 8.3 dB. The RMS spectral width of the laser in 40 Gbps and 100 Gbps Ethernet is required to be below 0.65 nm [34, Sec. 6].

In contrast to the Ethernet, the Fibre Channel standard is focused on high-speed short-range network technology primarily used to connect computer data storage. It is standardized in the T11 Technical Committee of the International Committee for Information Technology Standards (INCITS), an American National Standards Institute (ANSI)-accredited standards committee [80]. The list standard documents governing the Fibre Channel is available on the website if the T11 committee [81] and are available for purchase from ANSI. Fibre Channel was primarily used in supercomputers, but has become a common connection type for storage area networks (SAN) in enterprise storage. Although the optical fiber is the primary medium, it can also run on twisted pair copper wire in addition to fiber-optic cables. Similarly to the Ethernet, operation at 850 nm, 1300 nm and also 1550 nm is foreseen [82]. The RMS spectral width requirement for 850 nm is similar to Ethernet, 0.57 nm. Interestingly, Reed-Solomon (RS) forward error correction (FEC) is considered for future versions of Fibre Channel.

Infiniband is also focused on short-range interconnect in HPC and SAN applications and also foresees use of both copper and fiber-optic cabling. It is standardized by the InfiniBand Trade Association (IBTA), which is an industry consortium established in 1999 [83]. The leading members of IBTA are IBM, Intel, Mellanox, Emulex, Oracle, HP, and Cray. The main purpose of InfiniBand is to provide a low-latency, high-bandwidth

interconnect with low processing overhead and suitable to carry multiple traffic types (such as clustering, communications, storage, management) over a single connection. Long-haul transmission of InfiniBand over WAN technologies is also possible [83]. The Infiniband standard is constantly evolving, the progression of single-lane data rates and availability to date has been:

- Single Data Rate (SDR) 2.5 Gbps,

- Double Data Rate (DDR) 5 Gbps,

- Quad Data Rate (QDR) 10 Gbps,

- Fourteen Data Rate (FDR) 14.0625 Gbps,

- Enhanced Data Rate (EDR) 25.78125 Gbps.

The single lanes can be aggregated together in units of 4 or 12. The latest additions to the standard, FDR and EDR are so far only defined with electrical interfaces. In contrast to the older data rate definitions they use 64b/66b encoding and FEC. The code used is shortened cyclic code with block length of 2112 bits and 2080 bits of payload. The code (2112, 2080) is guaranteed to correct an error burst of up to 11 bits per block, which corresponds to to a BER of roughly 5×10^{-3} [84]. Active optical and active electrical cables are foreseen by the standard. For the connected optical interfaces two versions are foreseen, 850 nm with MMF for reach up to 300 m with 2000 MHz×m OFL bandwidth fiber and 1300 nm for up to 10 km with SMF. The only modulation format foreseen is OOK. In the 850 nm optical link the power budget is 6.25 dB, with average transmitted power of −2 dBm and maximum allowed laser RIN of −122 dB/Hz [84].

The given link power budgets are an important consideration for development and use of multilevel modulation formats in short-range optical links. The general trade-off is that higher spectral efficiency requires higher received optical power. The available power budgets are constrained by eye safety and VCSEL output power and power consumption considerations. Although it can be argued that e.g. eye safety is not relevant for active optical cables, the two other constraints are still present. What may make introduction of multilevel formats much easier from power budget perspective is introduction of the FEC, and this seems to be the directions where the standards are heading. Moreover, multilevel modulation in short-range optical modulation is a topic under debate in standardization committees.

3 Modulation

As the speed of the short-range optical connections is increasing, they become increasingly limited by the component bandwidth and modal dispersion in the MMF, which limits the usable distances. In this case, the industry has turned to parallel interconnects, such as those defined in the IEEE 802.3-2012 standard, in which 40 Gbps and 100 Gbps links are created by aggregation of 10 Gbps links. In effect, each link uses eight or twenty fibers in parallel, since a pair of fibers is needed for bi-directional communication. This has an advantage of keeping the transmission distances reasonably long, but it has the disadvantage of increasing the physical size of the interconnects. New designs reducing the size of the interconnects are being developed [85, 86]. Multilevel modulation formats can be used to increase the bit rate in each of the parallel lines, multiplying the achievable throughput. The increased spectral efficiency would primarily enable squeezing more data into the limited electrical bandwidth, without increasing the number of lasers, detectors, drivers and so forth.

There are however some constraints to consider - the typical link power budgets and wall-plug power consumption are limited. This means, that a modulation format with high spectral efficiency, good sensitivity and low complexity is needed. It is very hard to optimize all the three conditions at the same time, especially in an IM/DD system, where the available signal space is limited by the non-negativity constraint.

The problem becomes easier, if we restrict ourselves only to two parameters at a time, for example spectral efficiency and complexity, or spectral efficiency and sensitivity. If implementation in the short term is considered, it is important to keep the modulation formats easy to realize at high speed, given the constraints of today's electronics. It is interesting though, to look beyond short term constraints and investigate what would be a

good modulation format to e.g. maximize the sensitivity, without keeping strict hardware constraints. While application of digital signal processing (DSP) at high speed is difficult and implies high power consumption today, Moore's law still applies, as of today, and new possibilities might emerge in the future. Analog electronic equalization was discussed for short-range applications using both OOK [87] and was shown practically in [50]. Multi-level modulation formats were discussed in [88, 89]. Electronic equalization is already used in commercial electrical cables, e.g. in the Q:Active$^{\text{TM}}$ active copper cables marketed by Intersil [90]. The electronic equalization reduces the requirements for quality of the copper cabling, increases the transmission distance and reduces the cost. When electronic equalization for OOK will become commonplace, the next step may likely be implementation of more advanced modulation formats. Advanced modulation schemes such as trellis coded 16-level PAM are used today in 10 Gbps Ethernet running over Cat6e and Cat7 twisted pair copper cables [34, Sec. 4].

Once the complexity constraints on the electronic processing are moved into a background plane, one can consider optimization of more advanced modulation formats for improved sensitivity in IM/DD systems.

In this work a broad spectrum of modulation formats is covered, from simple modulation formats such as PAM, interesting for high-speed applications, through moderately complex and somewhat inefficient classical subcarrier formats to an interesting class of highly sensitive three-dimensional subcarrier formats. These will be discussed separately below. Other signal spaces based on different basis functions can be proposed, as long as the non-negativity constraint is fulfilled. An example of such a modulation format is pulse position modulation, which is commonly used in wireless infrared communications [79]. This type of modulation is very power efficient, but has rather poor spectral efficiency, so prospects of use in links based on MMF are weak. Bandlimited intensity modulation formats were investigated in [91]. Recently a modulation format called carrierless amplitude and phase (CAP) modulation was studied in MMF based applications [92–94]. The CAP modulation is related to the subcarrier modulation techniques. The main difference between CAP and subcarrier modulation is the use of additional pulse shaping (usually with a root-raised-cosine filter) on top of the sinusoidal basis functions of ordinary subcarrier modulation [95, 96].

3.1 Pulse amplitude modulation

Pulse amplitude modulation is the simplest modulation format applicable for IM/DD systems, such as short-range optical communications. In fact, OOK is a special case of PAM, with 2 modulation levels, each representing one bit. There is only one basis function in PAM, in the simplest case it is just a rectangular pulse,

$$\Phi_0(t) = \frac{1}{\sqrt{T}}\text{rect}(t/T), \tag{3.1}$$

where T denotes symbol time duration. For an M-level PAM the symbol waveforms may be represented as

$$s_m(t) = A_m\phi_0(t), \tag{3.2}$$

where $1 < m < M$. Note that this describes the optical intensity profile of the pulse, rather that the electrical field amplitude. The non-negativity constraint means also that negative values of s_m are not allowed and therefore all A_m values must be positive. An illustration of constellation diagrams
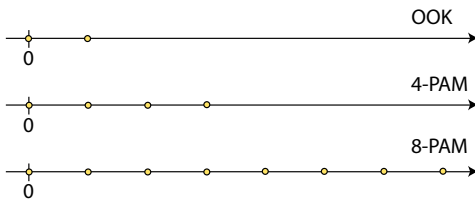

Figure 3.1: Constellation diagrams of OOK, 4-PAM and 8-PAM in an system with a non-negativity constraint.
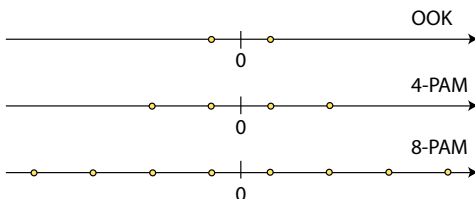

Figure 3.2: Constellation diagrams of OOK, 4-PAM and 8-PAM in an system without a non-negativity constraint.
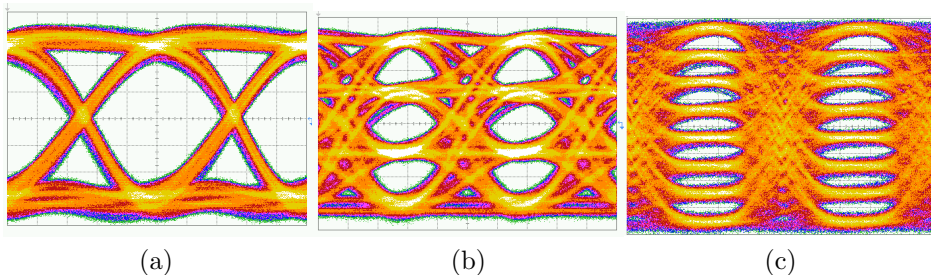
Figure 3.3: Experimental 2-, 4- and 8-PAM eye diagrams.

for OOK, 4-PAM and 8-PAM is shown in Fig. 3.1. Since there is only one basis function, the constellation diagram can be presented on one axis. For comparison, constellation diagrams of conventional PAM in systems without non-negativity constraint are included in Fig. 3.2.

It is also easy to illustrate the PAM modulation in the time domain. Examples of experimental OOK, 4-PAM and 8-PAM eye diagrams are illustrated in Fig. 3.3. Eye diagrams are simple and useful tools for getting a quick overview of signal quality and impairments in the system. Both SNR and timing jitter can be observed from eye diagrams. Lower SNR is manifested by broadened signal levels, and timing jitter is manifested by the widened eye crossings. It is also obvious from the eye diagrams that the more modulation levels there are, the higher is the required SNR to achieve error-free data transmission.

3.1.1 Theoretical BER calculation

As the number of modulation levels is increased, the spectral efficiency increases. If the bit rate is kept fixed, the bandwidth of M-level PAM is reduced by a factor of $\log_2(M)$, compared to OOK [97]. Alternatively, the symbol rate and bandwidth can be kept fixed and the bit rate increased. In either case, M-PAM will require more optical power at the receiver to reach the same BER than OOK.

It is useful to have an analytical expression for the expected system BER, as a function of the received optical power. Knowledge of the theoretically expected performance enables not only comparison with other modulation formats, but also proper evaluation of the experimental results and implementation penalties. Detailed derivation of the theoretical BER
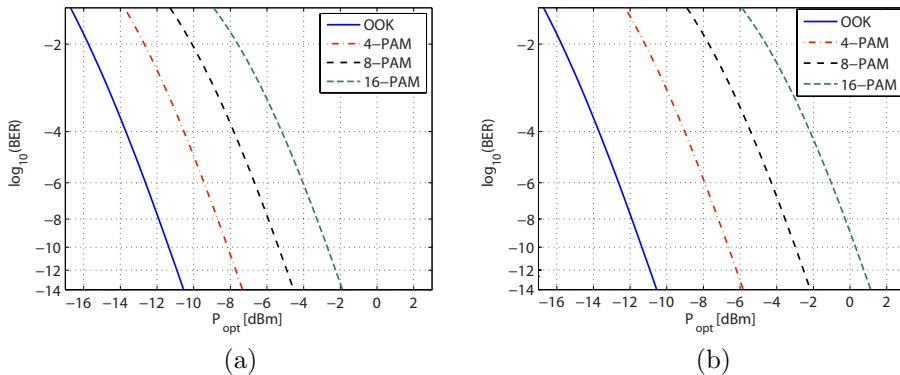
Figure 3.4: Theoretical bit error rates for 2-,4-,8- and 16-PAM at 20 Gbps (a) and at 20 Gbaud (b).

expression is presented in Paper F. If the SNR is high and the noise is Gaussian, the BER can be approximated as

$$BER \approx \frac{M-1}{M} \frac{d_{\mathrm{avg}}}{\log_2 M} \operatorname{erfc}\left(\frac{I_{\mathrm{avg}}}{(M-1)\sigma\sqrt{2}}\right) \qquad (3.3)$$

where I_{avg} is the average photocurrent, σ is the noise variance and d_{avg} is the average Hamming distance between the labels of adjacent symbols. If Gray labeling is used, $d_{avg} = 1$. If natural labeling is used it is given by

$$d_{avg} = 2 - \frac{\log_2(M)}{M-1}. \qquad (3.4)$$

In the case when the bit rate is fixed and the modulation order is increased the optical power penalty for using M-level PAM, compared to OOK, expressed in dB is

$$P_{pb} = 10\log_{10}\left(\frac{M-1}{\sqrt{\log_2(M)}}\right), \qquad (3.5)$$

where M is the number of modulation levels [97], this can be see in Fig. 3.4a. If the symbol rate is fixed, the optical power penalty compared to OOK is [98]

$$P_{ps} = 10\log_{10}(M-1), \qquad (3.6)$$

35

which can be seen in Fig. 3.4b. Obviously, there is a trade-off between power efficiency and bandwidth efficiency. On the other hand, if high speed components such as integrated photoreceivers are not available, then the penalty for use of photodetectors with voltage amplifiers, rather than transimpedance amplifiers outweighs the power penalty due to increased number of levels. Such a case was illustrated in Paper G, where 4-PAM at 25 Gbps, detected with 12 GHz photoreceiver was demonstrated to have around 1 dB sensitivity advantage over OOK detected with a 25 GHz photodetector, followed by a discrete voltage amplifier.

Because of the relaxed bandwidth requirements on components, multilevel PAM modulation can be useful in extending the transmission distance. In fact, PAM was proposed also for increasing the transmission distance in SMF [97] and along with equalization for electrical backplane connections [99]. In short-range applications PAM, in particular with 4 levels has been discussed in the context of polymer fiber links [100, 101]. The possibilities of implementation, advantages and drawbacks of PAM applications in MMF and VCSEL based links were studied in [88, 102, 103].

A study of 4-PAM application in short-range optical links is presented in Papers F and G. The knowledge of the theoretical performance was also useful in estimation the implementation penalties in experimental demonstration of 8-PAM in Paper I.

3.1.2 Effects of RIN on PAM

It is clear how the BER depends on the received optical power, if the main noise source is the thermal noise, which in general is additive, white and Gaussian. It is not always the thermal noise dominates. The system performance can be dominated by e.g. RIN originating in the laser, which is dependent on the received optical power. In this case, increasing the optical power into the receiver does not mean that a lower BER will be reached because the increase received signal power will be accompanied by higher noise power. The effects of RIN can be evaluated analytically, by taking it into account in the noise variance when calculating the BER. Examples of analytically calculated BER curves for OOK with 20 GHz noise bandwidth and RIN ranging from -150 dBm/Hz to -115 dBm/Hz are shown in Fig. 3.5a. Examples of BER curves for 4-PAM, also with 20 GHz noise bandwidth, with RIN in range from -150 dBm/Hz to -125 dBm/Hz are included in Fig. 3.5b. It was assumed that the decision thresholds are equidistant from the adjacent symbol levels. As the RIN levels are
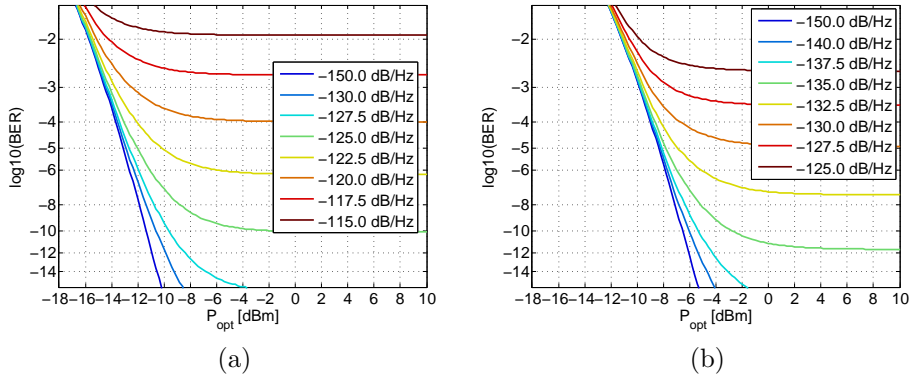
Figure 3.5: Influence of RIN on expected BER, shown for OOK(a) and 4-PAM (b) for 20 Gbaud symbol rate and 20 GHz bandwidth.

increased, the BER curves start showing progressively higher error floors. Naturally, an increased number of levels reduces the RIN level that can be tolerated. For better clarity the effects of RIN can be also quantified by the sensitivity penalty as a function of RIN. Sensitivity penalties due to RIN are shown in Figs. 3.6a and 3.6b for OOK and 4-PAM respectively, with noise bandwidths of 10, 20, 30 and 40 GHz. The theoretical penalties presented in Fig. 3.6a show that the highest acceptable RIN spectral density for high speed OOK operation is below −135 dB/Hz. The corresponding number for 4-PAM is −145 dB/Hz. For comparison, the VCSELs used in the experiments in the Papers A-H had RIN below −155 dB/Hz.

3.1.3 Intersymbol interference

Intersymbol interference (ISI) occurs when one symbol interferes with subsequent symbols. The sampled received signal values have a form [77, Ch. 9.2]

$$y_k = I_k x_0 + \sum_{\substack{n=0 \\ n \neq k}}^{\infty} I_n x_{k-n} + \nu_k, \tag{3.7}$$

where I_n denotes the transmitted symbols, x_n denotes the response of the system, and ν_k is the noise variable. The desired term, corresponding to the transmitted symbol is represented by I_k, the term x_0 can be treated as a scaling factor. The second term on the right hand side of Eq. 3.7 is the

undesired interference.

The effects of ISI on PAM signals can be visualized using an eye diagram. An example simulated 4-PAM eye diagram after transmission through a channel with Gaussian impulse response with a 3 dB bandwidth three times higher than the symbol rate is show in Fig. 3.7a. For comparison, an eye diagram of the same format, but in a channel with 3 dB bandwidth equal to 0.6 of the symbol rate is shown in Fig. 3.7b. There are two kinds of penalties introduced by the ISI, power penalty and timing penalty. Power penalty is due to the vertical eye closing, and the timing penalty is due to the horizontal eye closing.

The power penalty due to the ISI is well understood for OOK systems. The basic ISI penalty calculation methods, have been outlined in [104]. The ISI power penalty, expressed in dB, for any PAM formats is

$$P_{ISI} = 10 \log_{10} \left(\frac{1}{1 - E_m} \right), \tag{3.8}$$

where E_m is the worst case eye closure. In case of OOK it is approximated as

$$E_{m,OOK} = 1.425 \exp \left(-1.28 \left(\frac{T}{T_C} \right)^2 \right). \tag{3.9}$$

The bit period is denoted as T and the channel $10\% - 90\%$ rise-time is denoted as T_C. This ISI penalty calculation method, which is valid under
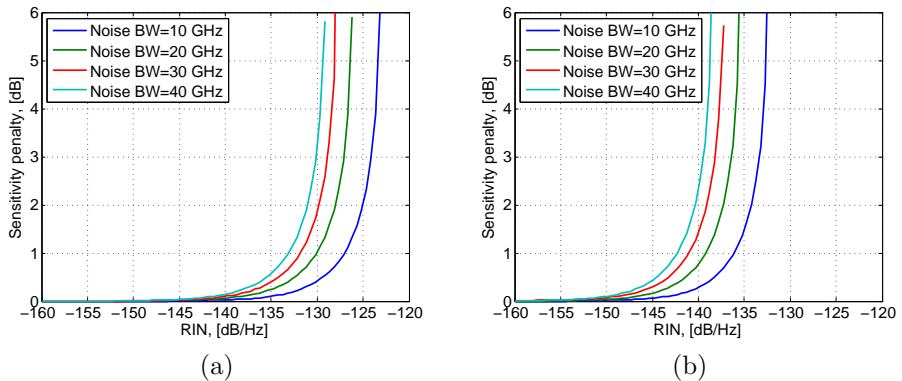
Figure 3.6: Sensitivity penalites due to RIN for OOK (a) and 4-PAM (a).
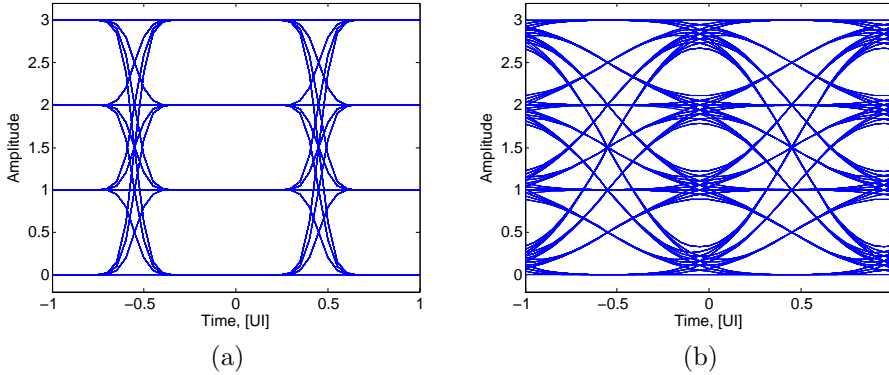
Figure 3.7: Simulated effects of ISI on a 4-PAM signal. On the left (a) the channel bandwidth is three times the symbol rate. One right (b) the channel bandwidth is 0.6 of symbol rate. In both cases Gaussian channel response is assumed.

assumption of a Gaussian channel response and rectangular input pulse, was given in [105]. It is used in the IEEE 802.3 link budget spreadsheet [106]. Methods of calculation of the $10\% - 90\%$ rise-time for a given system
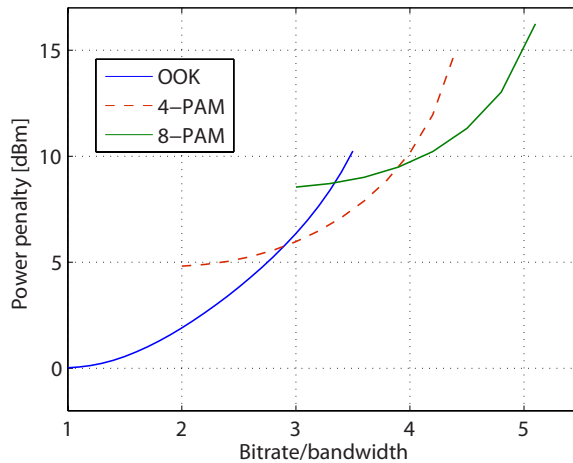
Figure 3.8: Sensitivity penalties including ISI for 2-,4-, and 8-PAM.

are described in [105].

The ISI penalty estimates can be extended to 4-PAM. A 4-PAM eye diagrams contains three OOK eye diagrams stacked on top of each other. Assuming that the channel response is Gaussian, it is easy to observe that for the same system rise-time and symbol rate, the eye closure in case of 4-PAM is twice as large as in the case of OOK,

$$E_{m,4PAM} = 2.85 \exp\left(-1.28\left(\frac{T}{T_C}\right)^2\right). \tag{3.10}$$

In the same manner, one can observe, that the eye closure in case of 8-PAM is

$$E_{m,8PAM} = 5.7 \exp\left(-1.28\left(\frac{T}{T_C}\right)^2\right). \tag{3.11}$$

In general, for an M-PAM format the eye closure will be

$$E_{m,MPAM} = \frac{M}{2}1.425 \exp\left(-1.28\left(\frac{T}{T_C}\right)^2\right). \tag{3.12}$$

In a simplistic view of a digital communication system if one wishes to increase the spectral efficiency, the only solution is to increase the number of modulation levels. In reality it may be easier and cheaper to increase the signaling rate beyond the channel 3 dB bandwidth and accept the resulting ISI penalty or to use equalizers. From the point of view of sensitivity, it is logical to switch to a higher order modulation format at the point when the ISI penalties for a lower order format are larger than the penalty for using more levels. This situation is illustrated in Fig. 3.8, where sensitivity penalties for OOK, 4-PAM and 8-PAM are plotted against the ratio of the data rate to the channel 3 dB bandwidth. The reference point for the power penalties is a sensitivity of and OOK system at data rate equal to the channel 3 dB bandwidth. The ISI penalties for OOK do not exceed the sensitivity penalty for going to 4-PAM until the point when the bit rate is three times larger than the system bandwidth. Similarly, the ISI penalties in case of 4-PAM do not exceed the sensitivity penalty for going to 8-PAM until the bit reaches 4 times the channel bandwidth. This theoretical model for ISI penalties was validated experimentally in Papers F and G.
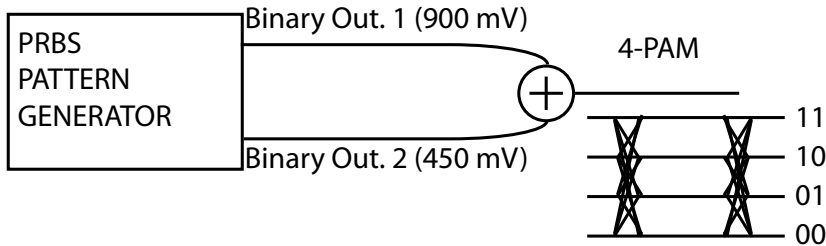
Figure 3.9: Generation of 4-PAM signal from two binary data streams.

3.1.4 Experimental techniques for PAM experiments

One of the advantages of PAM is the simplicity of implementation. In fact CMOS circuits operating at bit rates up to 22 Gbps have already been developed [107]. In a laboratory environment PAM signal can be generated in real time from binary signals. It is particularly simple for 4-PAM which can be generated by combining two clock aligned decorrelated binary data streams. One of the streams must be half of the amplitude of the other to get 4-PAM at the output. An example of a 4-PAM generating setup is illustrated in Fig. 3.9. This method of 4-PAM signal generation was used e.g. in the experiments presented in Paper H where 60 Gbps real-time 4-PAM was demonstrated. Generation of 8-PAM signal with this method is difficult. Conceptually, only one more binary signal source is required, as illustrated in Fig. 3.10. In reality, the signal quality generated with such a setup suffers from reflections in the power combiners. Precise signal phase control and amplitude is also required. A much better way to generate the 8-PAM signal is to use a dedicated circuit, such as an 8-bit digital to analog converter (DAC). This method was used in the experiments presented in Paper I

Experimental BER measurements can be also done in real time using a standard error analyzer designed for OOK. The decision threshold has to be set between the levels of 4-PAM and the error analyzer has to be programmed with a binary pattern corresponding to transitions of given PAM decision threshold. If the measured BER is low, it can be assumed that only symbol errors between neighboring levels occur. Thus, the calculation of the resulting BER can be greatly simplified. A thorough explanation of the real time BER measurement is presented in Paper E. In short, if the
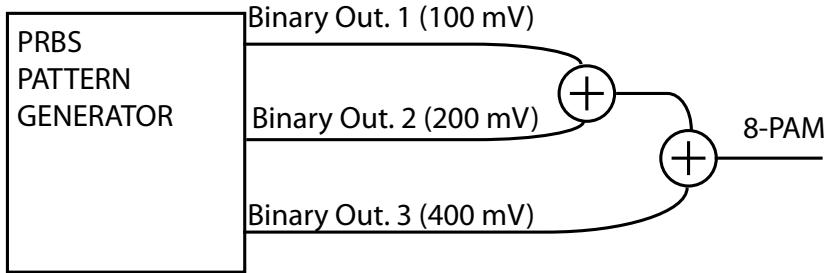
Figure 3.10: Generation of 8-PAM signal from three binary data streams.

error rates measured at the three decision thresholds are denoted as ER_1, ER_2, and ER_3, the total BER is given by

$$BER = \frac{1}{2}ER_1 + ER_2 + \frac{1}{2}ER_3, \tag{3.13}$$

which is valid only for natural labelling. This method of BER measurements was used in experiments with 4-PAM reported in Papers E and H. The highest achieved bit rate for which this BER measurement technique was used was 60 Gbps, reported in Paper H. This method is also adaptable to 8-PAM BER measurements, as it was demonstrated in Paper I. An alternative to this method would be to use a real-time sampling oscilloscope to capture the received waveform and calculate the BER off-line. The error analyser based approach has the distinct advantage of enabling BER measurements down to 10^{-12}, which is important for data communications applications. The lowest BER that can be reached using off-line processing in a reasonable time (less than 24 hours) is around 10^{-7}. The ability to reach low BER is important because until recently FEC was not accepted in datacomm applications. On the other hand, off-line BER measurement would be advantageous in case higher-order PAM, with 8 and more levels, since the manual adaptation of the threshold for each measurement is time consuming.

3.2 Subcarrier modulation

For subcarrier modulation, the intensity of the light is modulated with a microwave subcarrier, which itself is modulated with QAM or PSK. An
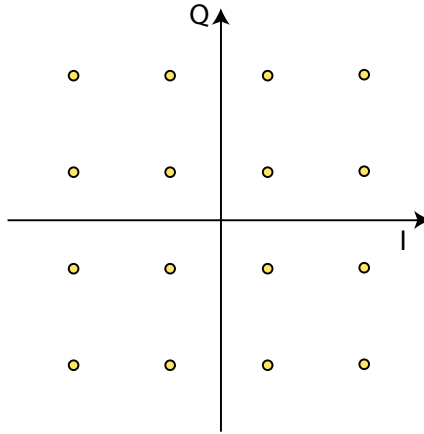
Figure 3.11: Constellation diagram of 16-QAM in the in-phase (I) and quadrature (Q) signal space.

advantage of the subcarrier modulation is that expertise in well-developed microwave technology can be leveraged. A technique called sub-carrier multiplexing is used in cable television systems for distribution of video signals, where each signal is carried on its own subcarrier [108], and it was also studied for broadband distribution [109]. The use of such a system is beneficial because optical fibers have much larger bandwidths and much lower losses than coaxial cables. On the other hand, the use of electronics to multiplex and de-multiplex the signal is a lower cost solution, compared to the use of photonic devices. There is also a related field of RF photonics, where photonic technology is used e.g. to transport and generate microwave signals.

Subcarrier modulation schemes can be roughly grouped into two categories, depending on the number of subcarriers. The first, simplest one comprises subcarrier schemes with only one subcarrier and with a carrier period equal to the symbol interval. Section 3.2.1 is devoted to single subcarrier modulation. The second group comprises schemes which involve multiple subcarriers. In multiple subcarrier schemes the subcarriers can be separated by guard bands, or be orthogonal. Section 3.2.3 is devoted to multiple subcarrier schemes.

3.2.1 Single-cycle subcarrier modulation

In the single-cycle single subcarrier modulation the period of the subcarrier is equal to the symbol interval. The basis functions of this modulation scheme are

$$\Phi_1(t) = \sqrt{\frac{2}{T}}\cos(2\pi ft)\text{rect}(t/T), \qquad (3.14)$$

$$\Phi_2(t) = \sqrt{\frac{2}{T}}\sin(2\pi ft)\text{rect}(t/T), \qquad (3.15)$$

where T is the symbol interval and $f = 1/T$ is the subcarrier frequency. The subcarrier can be modulated with any of the modulation formats using the in-phase and quadrature (I/Q) signal space. The modulated subcarrier is used to modulate the intensity of the light which can be detected with a simple photodiode at the receiver. Since the intensity cannot be negative, the whole signal has to be biased to avoid clipping. In the experiments described in Paper A a bias-T was used to provide the bias current for the VCSEL and to make the subcarrier signal non-negative. The driving bias current and subcarrier signal amplitude have to be selected to fit into the dynamic range of the VCSEL to avoid signal distortion. The single-cycle subcarrier modulation was investigated theoretically for general IM/DD systems, including free-space optical communications in [78, 79, 110] and demonstrated experimentally in fiber-optic systems in [111, 112]. An example of a 16-QAM constellation diagram in the signal space given by Φ_1 and Φ_2 is illustrated in Fig. 3.11. If square-shaped pules are used, the bandwidth of the main lobe of the signal spectrum is twice the symbol rate, because upper and lower side bands are imposed on the subcarrier. Therefore M^2-QAM used with single-cycle subcarrier modulation has the same spectral efficiency as M-PAM [110]. On the other hand, compared to PAM modulation with the same spectral efficiency and bandwidth, single-cycle subcarrier modulation will have half the symbol rate, which reduces the bandwidth requirements and makes digital processing and equalization easier. In experiments, single-cycle subcarrier modulation can be implemented either with microwave mixers, using DSP and DACs, or with XOR logic gates. A schematic showing real time generation of 16-QAM single-cycle subcarrier signal with XOR gates is shown in Fig. 3.12. The clock signal performs the function of a microwave subcarrier. If synchronous clock and binary data are fed to an XOR gate, it will either reproduce the input carrier, or produce an inverted version, depending on the data bit.
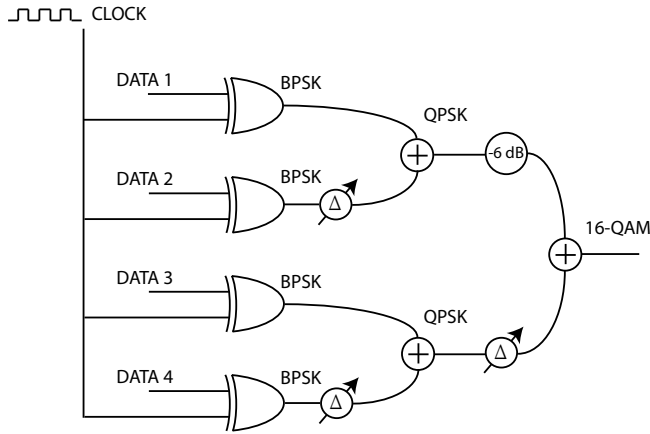
Figure 3.12: High speed 16-QAM single-cycle subcarrier generation based on XOR gates [113].

In this way a binary phase-shift keying (BPSK) signal is formed. Since all electronic components have finite bandwidth, the rectangular waveform output of the XOR gates is low pass filtered and thus becomes BPSK signal with sinusoidal carrier. Combining two BPSK signals, shifted by $\pi/2$ yields quadrature phase-shift keying (QPSK). Combing two phase aligned QPSK signals, with one having half of the amplitude of the other, yields 16-level QAM modulation. This method of single-cycle subcarrier generation was used in work presented in Paper A, where 37 Gbps transmission was demonstrated using single-cycle subcarrier modulation, over a link comprising a 20 GHz VCSEL and MMF.

The BER measurements of subcarrier modulation are more difficult to implement than for PAM modulation. Because there are two dimensions to be resolved, the demodulator is more complex than a simple threshold device. A demodulator structure is illustrated in Fig. 3.13. In Paper A the processing on the receiver side was implemented off-line. The received signal was sampled using a digital sampling oscilloscope, and the data was processed on a personal computer. This has imposed a limitation on the lowest measurable BER to around 10^{-6}. The actual symbol rate was 10 Gbaud, yielding 40 Gbps uncoded bit rate, but 7% overhead for FEC had to be accounted for, yielding usable bit rate of 37 Gbps. There are two gen-
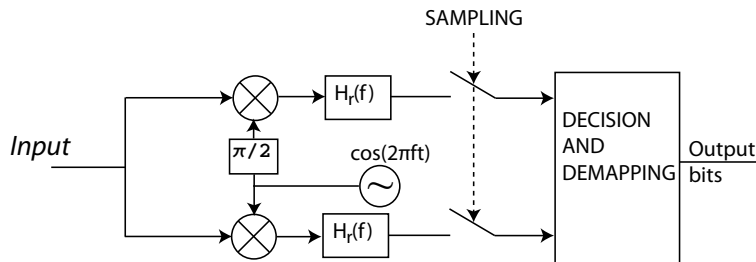
Figure 3.13: Demodulator for single subcarrier QAM.

eral disadvantages of conventional (i.e utilizing only the I/Q signal space) single subcarrier modulation, compared with 4-PAM; the first one is increased complexity and the second is a reduced sensitivity. Compared at the same spectral efficiency, the sensitivity of subcarrier M^2-QAM is 1.5 dB worse than corresponding M-PAM [114], mainly due to increased bias requirements.

3.2.2 Sub-cycle subcarrier modulation

The basis functions Φ_1 and Φ_2 given the Eq. 3.14 and the Eq. 3.15 can be defined for any value of f, also when $f < 1/T$. In this case, the single-cycle modulation becomes a sub-cycle subcarrier modulation, with a fraction of the carrier period per symbol period. The advantage of such arrangement of symbol and carrier periods is improved spectral efficiency of the modulation scheme, compared to single-cycle subcarrier modulation. Experimental demonstrations of sub-cycle subcarrier modulation with half-cycle subcarrier modulation in VCSEL and MMF based links were reported in [115]. Quarter-cycle subcarrier modulation in VCSEL based IM/DD link using SMF and 1550 nm wavelength was reported in [116, 117]. The half-cycle subcarrier modulation concept was applied also in SMF links with IM/DD [118, 119]. It was also demonstrated with dispersion compensation in [120]. The sub-cycle subcarrier modulation can be implemented using any of the methods suitable for single-cycle subcarrier modulation.
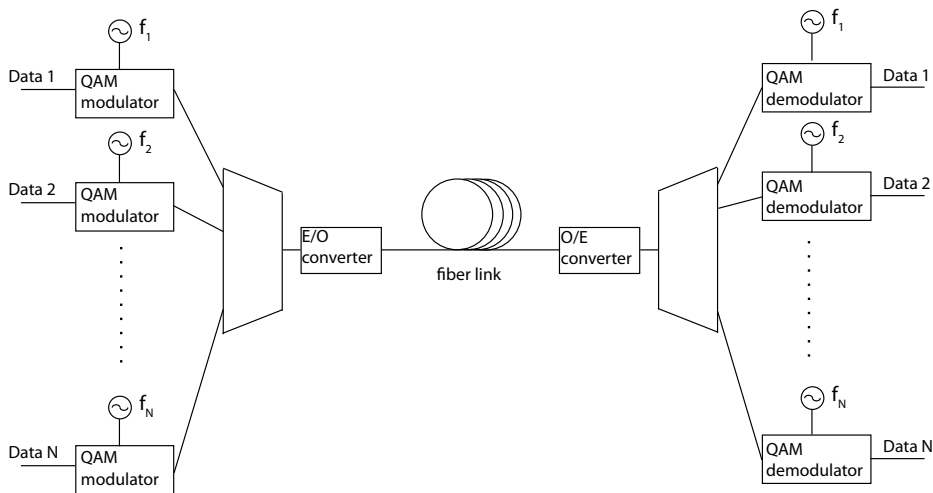
Figure 3.14: Subcarrier multiplexing scheme.

3.2.3 Multiple subcarrier modulation schemes

Although single subcarrier systems were considered in the previous section, the number of subcarriers may well increase. The multiple subcarriers can be orthogonal, although it is not necessary. Systems with multiple non-orthogonal subcarriers have been used for broadband access and TV signal distribution [46]. Non-orthogonal subcarriers, if sufficiently spaced, are easier to de-multiplex and are used to perform frequency division multiple access. A generic layout of a subcarrier multiplexing scheme is illustrated in Fig. 3.14. The multiple sub-carriers can also be orthogonal to each other, in a scheme called orthogonal frequency division multiplexing (OFDM) [77, Ch. 11.2]. In OFDM the subcarriers are separated in frequency by $\Delta f = 1/T$, where T is the symbol interval, which is the same on each subcarrier. The subcarriers are then orthogonal over the symbol interval. Practical implementations of OFDM are often based on fast Fourier transform [77, Sec. 11.2-5]. Application of OFDM in optical communications was discussed in [121]. In IM/DD system a particular form of OFDM is commonly applied – the discrete multi-tone modulation (DMT). In DMT, which was originally proposed for use in copper based links [122, 123], the output of the Fourier transform is real rather than complex. The latter is the case in conventional OFDM. The application of DMT in optical links

with MMF was studied in [124], and in [125] transmission of 30 Gbps over 500 m of MMF was demonstrated. The same technique was also applied to links with polymer fibers and transmission at bit rate of 47.7 Gbps was demonstrated [126].

The main motivation for application of DMT in short-range optical links is to combat the modal dispersion [124]. With OFDM and DMT it is possible to implement adaptive bit loading, providing for optimum power distribution over the subcarriers. On the other hand, the power efficiency of multiple subcarrier schemes is often poor. For a system with N subcarriers $5 \log_{10}(N)$ more received optical power is required, compared to single sub-carrier modulation, to reach the same BER [79]. There are also problems associated with high PAPR, imposing higher linearity requirements. Several methods of reduction of PAPR for multiple subcarrier schemes have been investigated [127, 128], and effects of clipping on OFDM performance have also been studied [121, 129]. It is also hard to implement DMT modulation in real time. The results reported in [125, 126] were obtained with off-line signal processing in both transmitter and receiver. A real-time implementation at 11.25 Gbps was reported in [130].

3.3   Three-dimensional subcarrier modulation

The power efficiency of modulation formats for IM/DD systems was studied in [78, 79, 110] and it was shown that classical subcarrier formats have

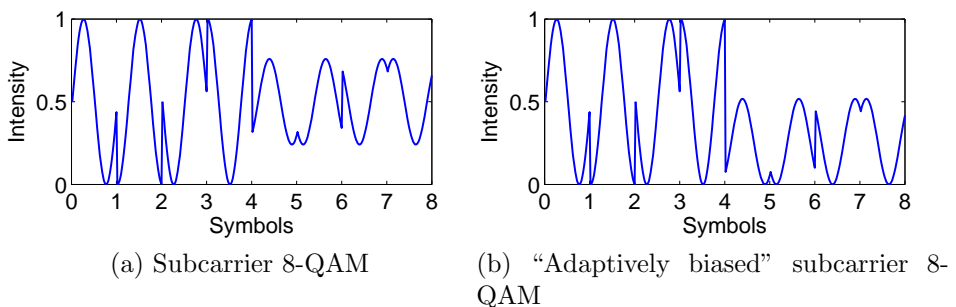(a) Subcarrier 8-QAM

(b) "Adaptively biased" subcarrier 8-QAM

Figure 3.15: Plot of intensity variations for classical subcarrier 8-QAM and adaptively biased 8-QAM.

worse sensitivity than PAM. The inefficiency stems from the fact, that given the non-negativity constraint in the IM/DD systems, the subcarrier signal in the optical domain has high average power. An example of 8-QAM subcarrier waveform is show in Fig. 3.15a and the corresponding constellation diagram is show in Fig. 3.16. For the subcarrier symbols with low amplitude, which in the constellation diagram are on the inner ring, there is a large amount of unmodulated optical power, which is essentially wasted. A simple measure to increase the efficiency is to reduce the bias of the symbols with low peak-to-peak amplitude. It can be seen as an improvement of the extinction ratio for these symbols. Example of an 8-QAM subcarrier waveform with this simple improvement is illustrated in Fig. 3.15b. This approach has been investigated in [78, 110] and was referred to as "adaptively biased QAM" (AB-QAM). In Paper C results of experimental work with AB-8-QAM are reported, 1 dB sensitivity improvement relative to conventional 8-QAM was demonstrated. However, some care must be taken to avoid misunderstanding. A "bias" is usually considered to be constant and the purpose of bias is usually to set the operating point for an electronic or optoelectronic device, here being a directly modulated laser. In the context of AB-QAM modulation in [78, 110], the term "bias" refers to symbol-by-symbol amplitude offset of the waveform. For consistency, the term "adaptive bias" will be used in this thesis the same manner as in [78, 110].

3.3.1 Three-dimensional signal space

One can observe that changing the amplitude offset of the subcarrier modulation gives a third degree of freedom in a subcarrier system. The subcarrier modulation can be therefore better described in a three-dimensional signal space given by the following basis functions:

$$\Phi_0(t) = \frac{1}{\sqrt{T}}\text{rect}(t/T), \tag{3.16}$$

$$\Phi_1(t) = \sqrt{\frac{2}{T}}\cos(2\pi f t)\text{rect}(t/T), \tag{3.17}$$

$$\Phi_2(t) = \sqrt{\frac{2}{T}}\sin(2\pi f t)\text{rect}(t/T), \tag{3.18}$$

where

$$\text{rect}(t) = \begin{cases} 1, & \text{if } 0 \le t < 1 \\ 0, & \text{otherwise} \end{cases},$$
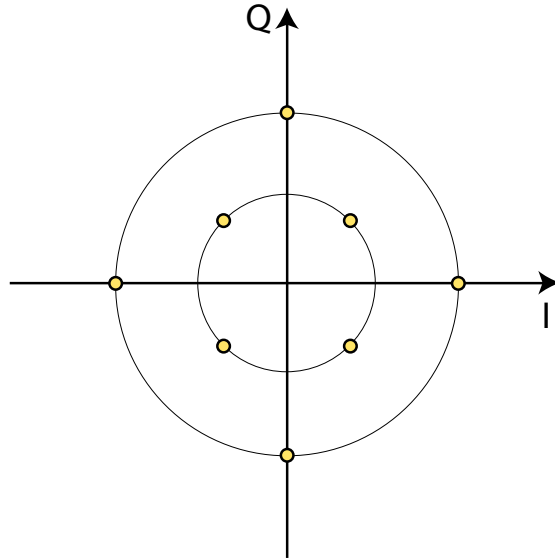
Figure 3.16: Star shaped 8-QAM constellation.

T is the symbol interval, and $f = 1/T$ denotes the subcarrier frequency, which is equal to the symbol rate. These basis functions were used in [78, 79] and in [131, Sec. 4.1-4.2]. The basis function Φ_0 is a rectangular pulse, which is a basis function of PAM. Thus, the signal spaces of PAM and subcarrier QAM are combined and both modulation types can be represented as special cases in this signal space. There is one significant constraint of the signal space – a requirement for the waveform non-negativity, since negative values of optical intensity are non-physical. The transmitted symbols of the subcarrier modulation are obtained by combining the three basis functions Φ_0, Φ_1, Φ_2 and the resulting linear combination must be positive, to be transmittable without clipping. The result of this constraint is that only a subset of the three-dimensional signal space is available. The admissible signal space is the interior of a cone with apex at the origin, opening into the dimensions spanned by Φ_0 and with apex angle of $\cos^{-1}(1/3) = 70.528^o$. A detailed analysis of the available signal space can be found in [78]. The available signal space, with an example of a 4-level modulation inscribed in it, is illustrated in Fig. 3.17.

Generation of the three-dimensional signals is fairly straightforward in practice. The basis functions Φ_1 and Φ_2 are already used in a conventional
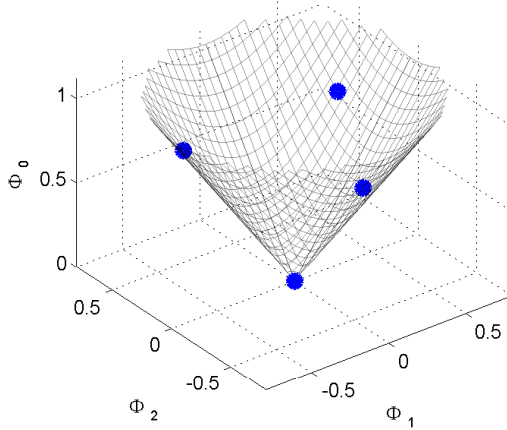
Figure 3.17: Three-dimensional constellation diagram of OOPSK modulation, inscribed in the conical admissible region.

I/Q modulator. What remains to be added, is the third branch corresponding to the adaptive symbol amplitude offset represented by Φ_0. The demodulator structure reflects the structure of the transmitter and comprises a conventional I/Q demodulator with additional branch for the Φ_0 basis function. The modulator and demodulator structures are illustrated in Fig. 3.18.

The three-dimensional modulation deserves some explanation in the

(a) Modulator   (b) Demodulator
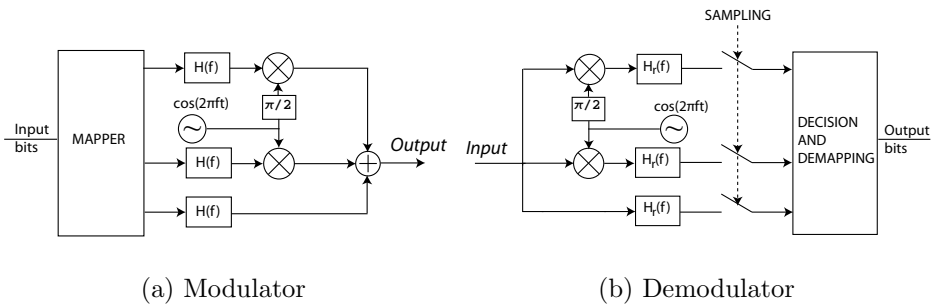
Figure 3.18: Modulator (a) and demodulator (b) structures for three-dimensional subcarrier modulation.

context of providing the right bias conditions for the directly modulated laser. The modulation signal and bias current are usually provided through a bias-T. A bias-T is a three port network, with one port passing direct current (DC) only, one port passing only high frequencies (HF) and a third port passing all. The bias current is provided through the DC port, the modulation is provided through the HF port and the laser is driven from the all-pass port. The basis functions in Eq. 3.16–3.18 describe how the current driving the laser, measured at the all-pass port of the bias-T looks, and consequently the intensity envelope of the light output of the directly driven laser. Needless to say, the non-negativity constraint cannot be satisfied at the input of the HF port of the bias-T, because any DC offset will be blocked, and any waveform passing through it will have an average value (calculated over many symbols) of 0. The non-negativity constraint must thus be satisfied after the DC bias current is added.

## 3.3.2 Modulation optimization in the three-dimensional signal space

With complete description of the signal space and the channel, it is possible to optimize the modulation formats for better optical power efficiency, electrical power efficiency or peak power. An example of a modulation format optimized for improved optical power efficiency for this signal space is a 4-level modulation format called on-off phase-shift keying (OOPSK), presented in [132]. The three-dimensional constellation diagram is shown inscribed in the three-dimensional signal space illustrated in Fig. 3.17. The predicted theoretical sensitivity is 0.6 dB better than for OOK and 2.1 dB better than for single-cycle subcarrier QPSK compared at the same bit rate. The theoretical predictions of performance of OOPSK in short-range links with VCSELs and MMF were confirmed experimentally in Paper B.

More examples of optimized subcarrier subcarrier formats can be found in [31] and [76]. An example of a simple improvement of the optical power efficiency was already illustrated in Fig. 3.15. In [31] it was shown that the 8-level AB-QAM (AB-8-QAM) has 1 dB better sensitivity than classical 8-QAM. Constellation diagrams of 8-QAM and AB-8-QAM in three-dimensional signal space are illustrated in Fig. 3.19a and Fig. 3.19b respectively. Spheres are used instead of points because they illustrate the minimum distance separation between the symbols.

Further optimization of the optical power efficiency can be done in the available signal space. Subcarrier formats in the three-dimensional signal
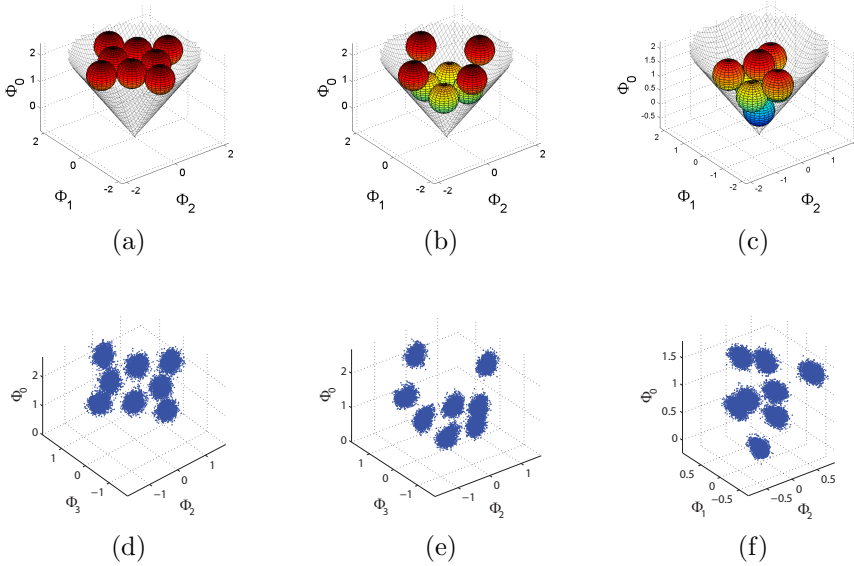
Figure 3.19: Constellation diagrams in three dimensions for 8-level subcarrier modulations – subcarrier 8-QAM (a), AB-8-QAM (b), 8-level subcarrier format optimized for electrical power(c), and respective experimental constellation diagrams (d–f).

space, optimized for optical power efficiency, electrical power efficiency and PAPR were also presented in [31]. The performance of 8-level formats optimized for optical power efficiency and electrical power efficiency is very close. Constellation diagram of a format optimized for the electrical power efficiency is illustrated in Fig. 3.19c. This modulation format has 2 dB better sensitivity than the 8-level QAM subcarrier modulation.

The performance of 8-level subcarrier formats was investigated experimentally and BER results are presented in Paper C. Constellation diagrams from the experiments are illustrated in Figs. 3.19d–3.19f.
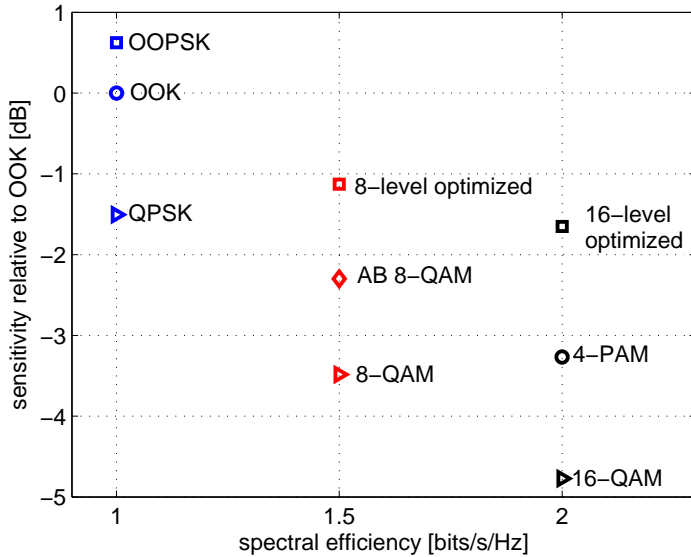
Figure 3.20: Comparison of sensitivity relative to OOK, for various investigated modulation formats [76].

3.4 Comparison of the modulation formats

Three types of modulation formats for IM/DD links were presented in this chapter PAM, subcarrier and three-dimensional subcarrier modulation. Direct experimental comparisons have been presented for some of the modulation formats, but not for all of them. This was partially due to a different focus – the objective of experiments with 4-PAM was to demonstrate high bit rates, while for experiments with three-dimensional subcarrier formats the goal was to demonstrate improved sensitivity. A theoretical comparison of all presented modulation formats was done in [76]. For comparison of performance of various modulation formats average optical power gain versus OOK was defined in [76]. For a given modulation format it is the sensitivity relative to OOK at the same bit rate. A plot of the relative sensitivity at high SNR, against the spectral efficiency, for the investigated modulation formats is presented in Fig. 3.20. A 16-level subcarrier modulation format optimized for power efficiency, proposed in [76], was also included. For given spectral efficiency, the subcarrier formats optimized

in the three-dimensional signal space have the best performance, but that comes as the expense of increased complexity. The simpler PAM formats perform worse, but are much easier to implement at high speed. Conventional subcarrier formats are neither efficient, nor easy to implement at high speed.

4 Future work and research utilization

4.1 Future and remaining work on PAM

The area of short-range optical interoconnects is developing very dynamically and is slowly moving towards more advanced technologies than OOK without FEC. New versions of the relevant standards include FEC and mutlilevel modulation will likely come next. Simple modulation formats, such as PAM have the highest chance of being adopted first. In this thesis some practical aspects of high-speed PAM were investigated, with greatest focus on sensitivity and effects of ISI on the sensitivity. This has been done in Papers E to I.

4.1.1 FEC

Application of FEC was investigated to some degree in Paper G. It was shown, that sensitivity of 25 Gbps 4-PAM system with FEC can be comparable to OOK without FEC at 12.5 Gbps. This means that link budgets of OOK systems can be preserved and it is very important, because of various reasons (e.g. eye safety) the transmitted optical power cannot be increase much above 0 dBm.

In Paper Gan RS code with 255 symbols long codewords and 239 payload data symbol was investigated. It is not the only possible code which can be used, and trade-offs for other relevant codes, with respect to error correcting capability, latency and power consumption, should be studied.

Coded modulation schemes are also an interesting possibility. Given that transmission over parallel fibers is often used, each fiber can be con-

sidered as a modulation dimension and a multi-dimensional coded modulation scheme could be considered. Such schemes are already used for Gigabit Ethernet over twisted pair copper cables [34, Sec. 4].

4.1.2 Timing jitter

Timing jitter is very important in practical applications, but in has not been studied in depth for PAM in short-range optical communication systems. It was only briefly investigated in Paper H for 50 Gbps 4-PAM. In this case the timing jitter was comparable to results reported for OOK at similar bit rate (e.g [50]). In studies of 4-PAM and OOK for copper back-plane interconnects it was shown that 4-PAM had lower timing margins than OOK. On the other hand, the frequency response of a typical short-range optical link is usually different from a backplane copper link response therefore it has to be researched, whether the timing jitter would be also a problem in optical systems. If it turns out to be a problem, an interesting question is whether method its mitigation can be devised (e.g. similar to [133]).

4.1.3 Equalization

Equalization of the ISI was not properly investigated, but it is already used in OOK based systems, e.g. in some 16 Gbps Fibre Channel transceivers [54]. An additional study including equalization of the ISI seems to be a natural follow-up to Paper G. It is not obvious, that the improvement in transmission distance due to equalization would be similar for e.g. OOK and 4-PAM.

4.1.4 Optimization of power consumption

The second most important question after how fast the data can be sent is how much power the transmission will require. Co-optimization of all the techniques mentioned before and making a trade-off with power consumption is a very important task, because the power consumption is the main cost of running a data center. Additionally, all wasted power is turned into heat, and heat rejection is a difficult problem. Co-optimization of the entire system from power and performance perspective is a challenging task, because it is an interdisciplinary challenge. It requires competence in optical communications, electronics design and information theory.

4.2 Application of the three-dimensional subcarrier formats

The modulation formats presented in Papers B-D are state-of-the-art when it comes to sensitivity at a given spectral efficiency. Although today high-speed implementations of such formats are difficult, they could become a feasible option in the future. Moreover, there are other areas where IM/DD is used, but high bit rates in order of tens of gigabits are not required, such as polymer fiber networks in automotive applications [134] or wireless optical networks [79].

Single subcarrier modulation does not have any significant advantage over PAM modulation or three-dimensional subcarrier modulation to warrant further work. It has worse sensitivity and nearly the same complexity as three-dimensional subcarrier modulation, and therefore, no further work is planned. On the other hand, multiple-subcarrier modulation formats are interesting, because each subcarrier contributes two dimensions – in-phase and quadrature. Optimization of modulation formats in such a multi-dimensional signal space is an interesting and mostly an open problem.

4.3 Areas of utilization

Throughout this thesis applications of the modulation formats in high-speed, short-range interconnects, such as those used in data centers were stressed, but the results can be and probably will be used beyond this field. As the optical links are reaching into new markets, such as consumer devices, industrial control networks, distribution of multimedia in automobile [134] and aviation [135] applications, the potential for utilization of the results of this work is increasing. The recent development of LED based lighting opens new possibilities of using them for sending data [136], e.g. to multimedia devices or for purposes of automation and control.

5   Contributions

Nine papers are included in the thesis. Papers A to D deal with subcarrier modulation formats and Papers E to I deal with PAM. A summary of the main contributions of the papers is presented below.

Paper A

In this paper experimental results with single-cycle subcarrier modulation were reported. The transmission system comprised a VCSEL with 20 GHz modulation bandwidth, OM3+ MMF and a photdiode with 25 GHz modulation bandwidth followed by a discrete amplifier. A symbol rate of 10 Gbaud was used, which with 16-QAM modulation yielded 40 Gbps data rate, but since the processing on the receiver side was implemented off-line, the BER was limited to 10^{-6}, so overhead for FEC had to be accounted for. The net reported bit-rate was 37 Gbps over 200 m of OM3+ type MMF. Although the receiver was implemented off-line, the transmitted was operating in real time.

My contributions: I set up the optical part of the experimental setup, performed the experiment and wrote the paper.

Paper B

In this paper a modulation format for an IM/DD system with the same spectral efficiency as OOK, but with better sensitivity was demonstrated. The new modulation format, called OOPSK, utilized the three-dimensional subcarrier signal space. The sensitivity was measured to be 0.6 dB better than for OOK. The experiments were performed with an IM/DD link com-

prising a VCSEL, OM3+ MMF and a photodiode for direct detection. For comparison, single-cycle subcarrier QPSK modulation was included, which was shown to have 1.5 dB worse sensitivity than OOK and 2.1 dB worse sensitivity than OOPSK. The modulation formats were compared at 5 Gbps bit-rate, and the processing was implemented off-line.

My contributions: I participated in the development of the OOPSK format, set up and performed the experiment, wrote the DSP code and wrote the paper.

Paper C

The concept of three-dimensional subcarrier modulation was extended to an 8-level subcarrier format. In this paper it was experimentally shown that the "adaptive bias" technique can improve the sensitivity of subcarrier star shaped 8-QAM by 1 dB. An optimized 8-level subcarrier format was experimentally shown to have 2 dB better sensitivity than the original star-shaped 8-level subcarrier modulation. The comparison of the modulation formats was done using an IM/DD system comprising a VCSEL, a short MMF patchcord an a photodiode. The comparison was performed at bit-rate of 7.5 Gbps, and the processing was implemented off-line.

My contributions: I set up and performed the experiment, wrote the DSP code and wrote the paper.

Paper D

In this paper the work three-dimensional subcarrier modulation formats is extended to 16-level formats. A 16-level three-dimensional format, optimized for optical and electrical power efficiency, under a constraint for a face-centred cubic lattice is experimentally demonstrated. The new format was show to have around 1 dB better sensitivity than 4-PAM and 2 dB better sensitivity than a single-cycle subcarrier 16-QAM.

My contributions: I set up and performed the experiment, wrote the DSP code and wrote the paper.

Paper E

In this paper results of experimental work with 4-PAM modulation are presented. Bit-rates as high as 30 Gbps using 4-PAM were demonstrated, along with a comparison of 25 Gbps transmission using 4-PAM and OOK. The transmission system comprised a VCSEL with 16 GHz modulation bandwidth, operating at wavelength of 850 nm, OM3+ MMF and 12 GHz photoreceiver for 4-PAM and 25 GHz photodiode for OOK. The maximum transmission distance in the OM3+ fiber was 300 m for 25 Gbps 4-PAM and 200 m for 30 Gbps 4-PAM. Only 200 m distance was reached with 25 Gbps OOK, demonstrating that 4-PAM can be used both to increase the bit-rates and to improve the transmission distance.

My contributions: I set up and performed the experiment and wrote the paper.

Paper F

This paper was focused on a comparison of 4-PAM and OOK in short-range optical links, using VCSELs operating at wavelength of 850 nm, OM3+ MMF and direct detection. Both experimental and theoretical comparisons were performed. The comparisons were performed at the same symbol rate for both modulation formats, and at the same bit-rate. Power budget requirements and propagation properties were investigated.

My contributions: I did the theoretical analysis of the M-PAM performance (with help from Erik Agrell), built the experimental setup, performed the experiments and wrote the paper.

Paper G

This paper presents results of experimental and theoretical investigation of intersymbol interference in 4-PAM transmission in short-range optical communications links based on the power penalty. The link under considerations comprised of a directly modulated 850 nm VCSEL with up to 200 m of MMF and direct detection was used. The link bandwidth was slightly below 10 GHz. Transmission results for 4-PAM and OOK were compared, with maximum achieved bit-rate of 44 Gbps in case of 4-PAM and 32 Gbps in case of OOK. FEC was also investigated, with a result that with a typical RS(255,239) code the sensitivity of the 4-PAM system would improve by

up to 4 dB, reaching 10 dBm at 25 Gbps.

My contributions: I did the theoretical analysis of the 4-PAM performance (excluding the parts about FEC which were contributed by Erik Agrell), built the experimental setup, performed the experiments and wrote the paper.

Paper H

In this paper transmission at record-high data rates using 4-PAM and a directly modulated 850 nm VCSEL was demonstrated. Transmission speeds of 60 Gbits over 2 m, 50 Gbits over 50 m and 40 Gbits over 100 m of OM4 MMF were achieved. In addition, the timing margins of high-speed 4-PAM were investigated for all threshold levels at 50 Gbps.

My contributions: I have built the experimental setup, performed the experiments and wrote the paper.

Paper I

In this contribution experimental demonstration of 8-PAM transmission using an 850 nm VCSEL and 100 m of OM4-type MMF was reported. The 8-level driving signal was generated using a 3-bit DAC, the error rates were measured in real time using a conventional error analyzer. Maximum uncoded bit rate was 37.5 Gbps, which would correspond to 35.2 Gbps with 7% FEC overhead.

My contributions: I have built the experimental setup, performed the experiments and wrote the paper.

Bibliography

[1] "Statistics of the International Telecommunications Union," available online `http://www.itu.int/en/ITU-D/Statistics/Pages/stat/default.aspx` accessed 2013-09-03.

[2] K. C. Kao and G. A. Hockham, "Dielectric-fibre surface waveguides for optical frequencies," *Proc. IEE*, 113(7):1151–1158, Jul. 1966.

[3] F. P. Kapron, D. B. Keck, and R. D. Maurer, "Radiation losses in glass optical waveguides," *Appl. Phys. Lett.*, 17(10):423–425, Nov. 1970.

[4] M. I. Nathan, W. P. Dumke, G. Burns, F. H. Dill, and G. Lasher, "Stimulated emission of radiation from GaAs p-n junctions," *Appl. Phys. Lett.*, 1(3):62–64, 1962.

[5] N. Holonyak and S. F. Bevacqua, "Coherent (visible) light emission from $Ga(As_{(1-x)}P_x)$ junctions," *Appl. Phys. Lett.*, 1(4):82–83, 1962.

[6] T. M. Quist, R. H. Rediker, R. J. Keyes, W. E. Krag, B. Lax, A. L. McWhorter, and H. J. Zeigler, "Semiconductor maser of GaAs," *Appl. Phys. Lett.*, 1(4):91–92, 1962.

[7] I. Hayashi, M. B. Panish, P. W. Foy, and S. Sumski, "Junction lasers which operate continuously at room temperature," *Appl. Phys. Lett.*, 17(3):109–111, Aug. 1970.

[8] S. B. Poole, D. N. Payne, R. J. Mears, M. E. Fermann, and R. Laming, "Fabrication and characterization of low-loss optical fibers containing rare-earth ions," *IEEE J. Lightw. Technol.*, 4(7):870–876, 1986.

[9] E. Desurvire, J. R. Simpson, and P. C. Becker, "High-gain erbium-doped traveling-wave fiber amplifier," *Opt. Lett.*, 12(11):888–890, Nov 1987.

[10] R. J. Mears, L. Reekie, I. M. Jauncey, and D. N. Payne, "Low-noise erbium-doped fibre amplifier operating at 1.54 μm," *Electron. Lett.*, 23(19):1026–1028, Sept. 1987.

[11] S. Saito, Y. Yamamoto, and T. Kimura, "Optical heterodyne detection of directly frequency modulated semiconductor laser signals," *Electron. Lett.*, 16(22):826–827, 1980.

[12] F. Favre, L. Jeunhomme, I. Joindot, M. Monerie, and J. Simon, "Progress towards heterodyne-type single-mode fiber communication systems," *IEEE J. Quantum Elect.*, 17(6):897–906, 1981.

[13] J. Kahn, "1 Gbit/s PSK homodyne transmission system using phase-locked semiconductor lasers," *IEEE Photon. Technol. Lett.*, 1(10):340–342, 1989.

[14] Ciena, "Wavelogic 3 coherent optical processors," available online `http://www.ciena.com/technology/wavelogic3/` accessed 2013-09-03.

[15] "VISIT project deliverable 5.1," available online `http://www.visit.tu-berlin.de/fileadmin/f23/VISIT_D5.1_PU.pdf` accessed 2013-09-10.

[16] J. Tatum, "VCSEL proliferation," *Proc. SPIE*, 6484:648403–648403–7, Jan. 2007.

[17] D. A. B. Miller, "Rationale and challenges for optical interconnects to electronic chips," *Proc. IEEE*, 88(6):728–749, 2000.

[18] M. A. Taubenblatt, "Optical interconnects for high-performance computing," *IEEE J. Lightw. Technol.*, 30(4):448–457, 2012.

[19] X. Wang, W. Jiang, L. Wang, H. Bi, and R. Chen, "Fully embedded board-level optical interconnects from waveguide fabrication to device integration," *IEEE J. Lightw. Technol.*, 26(2):243–250, 2008.

[20] M. Schneider and T. Kühner, "Optical interconnects on printed circuit boards using embedded optical fibers," *Proc. SPIE*, 6185:61850L–61850L–8, Apr. 2006.

[21] B. Jalali and S. Fathpour, "Silicon photonics," *IEEE J. Lightw. Technol.*, 24(12):4600–4615, 2006.

[22] M. Zuffada, "The industrialization of the silicon photonics: Technology road map and applications," in *Proc. ESSDERC*, 2012.

[23] Corning, "Thunderbolt active optical cables," available online `http://www.corning.com/CableSystems/OpticalCablesbyCorning/products/thunderbolt.aspx#.UkrstzZgc40` accessed 2013-09-30.

[24] J. Loehr, W. Siskaninetz, J. Wiemeri, and S. Feld, "Optical communication systems for avionics," *IEEE Aerosp. Electron. Syst. Mag*, 13(4):9–12, 1998.

[25] Y. Chen, H. Hemmati, and R. Some, "Multi-Gb/s fiberoptic physical layer for spacecraft interconnects," *IEEE J. Lightw. Technol.*, 31(12):1899–1905, 2013.

[26] E. Murphy, C. Michie, H. White, W. Johnstone, A. Kelly, and I. Andonovic, "High temperature wavelength division network for avionic applications," *IEEE J. Lightw. Technol.*, 31(18):3006–3013, 2013.

[27] "IEEE standard for information technology telecommunications and information exchange between systems local and metropolitan area networks specific requirements," available online `http://standards.ieee.org/findstds/standard/802.3ba-2010.html` accessed 2013-09-30.

[28] D. Molin, M. Astruc, and P. Sillard, "Chromatic dispersion compensated multimode fibers for data communications," in *Proc. ECOC*, paper Tu.3.C.3, Sept. 2011.

[29] R. Safaisini, K. Szczerba, E. Haglund, P. Westbergh, J. S. Gustavsson, A. Larsson, and P. A. Andrekson, "20 Gbit/s error-free operation of 850 nm oxide-confined VCSELs beyond 1 km of multimode fibre," *Electron. Lett.*, 48(19):1225–1227, 2012.

[30] R. Safaisini, K. Szczerba, P. Westbergh, E. Haglund, B. Kögel, J. S. Gustavsson, M. Karlsson, P. Andrekson, and A. Larsson, "High-speed 850nm quasi-single-mode VCSELs for extended-reach optical interconnects," *J. Opt. Commun. Netw.*, 5(7):686–695, Jul 2013.

[31] J. Karout, E. Agrell, K. Szczerba, and M. Karlsson, "Designing power-efficient modulation formats for noncoherent optical systems," in *Proc. Globecom*, Dec. 2011.

[32] C. Shannon, "A mathematical theory of communications," *Bell Systems Technical Journal*, 27:379–423 and 623–656, 1948.

[33] P. Westbergh, R. Safaisini, E. Haglund, J. S. Gustavsson, A. Larsson, and A. Joel. "High-speed 850 nm VCSELs with 28 GHz modulation bandwidth for short reach communication,", 2013.

[34] "IEEE standard for ethernet," available online `http://standards.ieee.org/about/get/802/802.3.html` accessed 2013-09-30.

[35] L. A. Coldren, S. W. Corzine, and M. L. Mashanovitch. *Diode lasers and photonic integrated circuits.* Wiley, 2012.

[36] K. Iga, S. Kinoshita, and F. Koyama, "Microcavity GalaAs/GaAs surface-emitting laser with I_{th} = 6 mA," *Electron. Lett.*, 23(3):134–136, Jul. 1987.

[37] I. Melngailis, "Longitudinal injection-plasma laser of InSb," *Appl. Phys. Lett.*, 6(3):59–60, 1965.

[38] H. H. E. Li and K. Iga. *Vertical-cavity surface-emitting laser devices*, volume 6. Springer, 2003.

[39] R. Michalzik. *VCSELs: Fundamentals, Technology and Applications of Vertical-Cavity Surface-Emitting Lasers.* Springer Series in Optical Sciences.

[40] C. Wilmsen, H. Temkin, and L. Coldren. *Vertical-Cavity Surface-Emitting Lasers: Design, Fabrication, Characterization, and Applications.* Cambridge University Press, 2001.

[41] S. Yu. *Analysis and Design of Vertical Cavity Surface Emitting Lasers.* Wiley, 2003.

[42] M. Amann, "Semiconductor lasers: Tuning triumph," *Nature Photon.*, 2(3):134–135, Mar. 2008.

[43] P. Moser, J. A. Lott, P. Wolf, G. Larisch, H. Li, N. N. Ledentsov, and D. Bimberg, "56 fJ dissipated energy per bit of oxide-confined 850 nm VCSELs operating at 25 Gbit/s," *Electron. Lett.*, 48(20):1292–1294, 2012.

[44] P. Moser, W. Hofmann, P. Wolf, J. A. Lott, G. Larisch, A. Payusov, N. N. Ledentsov, and D. Bimberg, "81 fJ/bit energy-to-data ratio of 850 nm vertical-cavity surface-emitting lasers for optical interconnects," *Appl. Phys. Lett.*, 98(23):231106, 2011.

[45] W. S. Chang. *RF photonic technology in optical fiber links*. Cambridge University Press, 2002.

[46] W. I. Way. *Broadband Hybrid Fiber Coax Access System Technologies*. Academic Press, Inc., Orlando, FL, USA, 1st edition, 1998.

[47] C. Carlsson, H. Martinsson, J. Vukusic, J. Halonen, and A. Larsson, "Nonlinear distortion and dynamic range of red (670 nm) oxide confined VCSELs," *IEEE Photon. Technol. Lett.*, 13(4):358–360, Apr. 2001.

[48] E. Haglund, A. Haglund, P. Westbergh, J. S. Gustavsson, B. Kögel, and A. Larsson, "25 Gbit/s transmission over 500 m multimode fibre using 850 nm VCSEL with integrated mode filter," *Electron. Lett.*, 48(9):517–519, 2012.

[49] P. Westbergh, E. Haglund, E. Haglund, R. Safaisini, J. Gustavsson, and A. Larsson, "High-speed 850 nm VCSELs operating error free up to 57 Gbit/s," *Electronics Letters*, 49(16):1021–1023, 2013.

[50] D. M. Kuchta, C. L. Schow, A. V. Rylyakov, J. E. Proesel, F. E. Doany, C. Baks, B. H. Hamel-Bissell, C. Kocot, L. Graham, R. Johnson, G. Landry, E. Shaw, A. MacInnes, and J. Tatum, "A 56.1 Gb/s NRZ modulated 850nm VCSEL-based optical link," in *Proc. OFC*, paper OW1B.5, 2013.

[51] P. Westbergh, J. S. Gustavsson, B. Kögel, Å. Haglund, A. Larsson, A. Mutig, A. Nadtochiy, D. Bimberg, and A. Joel, "40 Gbit/s error-free operation of oxide-confined 850 nm VCSEL," *Electron. Lett.*, 46(14):1014–1016, Jul. 2010.

[52] W. Hofmann, P. Moser, P. Wolf, A. Mutig, M. Kroh, and D. Bimberg, "44 Gb/s VCSEL for optical interconnects," in *Proc. OFC*, paper PDPC5, Mar. 2011.

[53] D. Gazula, J. K. Guenter, R. H. Johnson, G. D. Landry, A. N. MacInnes, G. Park, J. K. Wade, J. R. Biard, and J. A. Tatum, "Emerging VCSEL technologies at Finisar," *Proc. SPIE*, 7615:761506–761506–8, 2010.

[54] Avago, "14 Gbps Fibre Channel transceivers," available online `http://www.avagotech.com/docs/AV02-2508EN` accessed 2013-10-09.

[55] M. Chacinski, N. Chitica, S. Molin, N. Lalic, and O. Sahlen, "25.78 Gbps data transmission with 850 nm multimode VCSEL packaged in QSFP form factor module," in *Proc. OFC*, paper OW1B.1, 2013.

[56] J. A. Tatum, D. Smith, J. K. Guenter, and R. H. Johnson. "High-speed characteristics of VCSELs,", 1997.

[57] B. E. A. Saleh and M. C. Teich. *Fundamentals of photonics.* Wiley, 1991.

[58] A. W. Snyder and J. Love. *Optical Waveguide Theory.* Springer, 1983.

[59] P. Pepeljugoski, S. E. Golowich, A. J. Ritger, P. Kolesar, and A. Risteski, "Modeling and simulation of next-generation multimode fiber links," *IEEE J. Lightw. Technol.*, 21(5):1242–1255, May 2003.

[60] R. Pimpinella and A. Brunsting, "Differential mode delay (DMD) for multimode fiber types and its relationship to measured performance," in *Proc. OFC*, paper NWF2, Mar. 2005.

[61] L. Raddatz, I. H. White, D. G. Cunningham, and M. C. Nowell, "Increasing the bandwidth-distance product of multimode fibre using offset launch," *Electron. Lett.*, 33(3):232–233, Jan. 1997.

[62] R. Olshansky, "Propagation in glass optical waveguides," *Rev. Mod. Phys.*, 51:341–367, Apr 1979.

[63] B. Franz and H. Bülow, "Experimental evaluation of principal mode groups as high-speed transmission channels in spatial multiplex systems," *IEEE Photon. Technol. Lett.*, 24(16):1363–1365, 2012.

[64] R. E. Freund, C. Bunge, N. N. Ledentsov, D. Molin, and C. Caspar, "High-speed transmission in multimode fibers," *IEEE J. of Lightw. Technol.*, 28(4):569–586, 2010.

[65] D. Gloge and E. A. J. Marcatili, "Multimode theory of graded-core fibers," *Bell Syst. Tech. J*, 52(9):1563–1578, 1973.

[66] N. N. Ledentsov, J. A. Lott, J.-R. Kropp, V. A. Shchukin, D. Bimberg, P. Moser, G. Fiol, A. S. Payusov, D. Molin, G. Kuyt, A. Amezcua, L. Y. Karachinsky, S. A. Blokhin, I. I. Novikov, N. A. Maleev, C. Caspar, and R. Freund, "Progress on single mode VCSELs for data- and tele-communications," *Proc. SPIE*, 8276:82760K–82760K–11, 2012.

[67] A. Sengupta, "Comparison of min-EMBc and DMD template based qualification of high bandwidth multimode fibers," in *Proc. IWCS*, pages 154–160, 2007.

[68] A. Sengupta, "Calculated modal bandwidths of an OM4 fiber and the theoretical challenges," in *Proc. IWCS*, volume 9, pages 24–29, 2009.

[69] A. M. E. A. Diab, J. D. Ingham, R. V. Penty, and I. H. White, "Statistical analysis of subcarrier-modulated transmission over 300 m of 62.5-μm-core-diameter multimode fiber," *IEEE J. Lightw. Technol.*, 23(8):2380–2398, Aug. 2005.

[70] A. Gholami, D. Molin, and P. Sillard, "Compensation of chromatic dispersion by modal dispersion in MMF- and VCSEL-based gigabit ethernet transmissions," *IEEE Photon. Technol. Lett.*, 21(10):645–647, 2009.

[71] N. N. Ledentsov, J. A. Lott, D. Bimberg, A. Mutig, G. Fiol, S. A. Blokhin, A. M. Nadtochiy, V. A. Shchukin, J. Kropp, I. I. Novikov, L. Y. Karachinsky, and M. V. Maximov, "High-speed single-mode

quantum dot and quantum well VCSELs," *Proc. SPIE*, 7952:79520J–79520J–9, 2011.

[72] ISO/IEC 11801:2002/Amd 2:2010. *Information technology - Generic cabling for customer premises.* ISO, Geneva, Switzerland, 2010.

[73] R. S. Quimby. *Photonics and Lasers.* Wiley, 2006.

[74] G. P. Agrawal. *Lightwave technology: telecommunication systems.* Wiley-Interscience, 2005.

[75] A. Valle and L. Pesquera, "Relative intensity noise of multitransverse-mode vertical-cavity surface-emitting lasers," *IEEE Photon. Technol. Lett.*, 13(4):272–274, Apr. 2001.

[76] J. Karout, E. Agrell, K. Szczerba, and M. Karlsson, "Optimizing constellations for single-subcarrier intensity-modulated optical systems," *IEEE. Trans. Inf. Theory*, 58(7):4645–4659, 2012.

[77] J. G. Proakis. *Digital communication.* McGraw-Hill, 2008.

[78] S. Hranilovič and F. R. Kschischang, "Optical intensity-modulated direct detection channels: signal space and lattice codes," *IEEE T. Inform. Theory*, 49(6):1385–1399, Jun. 2003.

[79] J. M. Kahn and J. R. Barry, "Wireless infrared communications," *Proc. IEEE*, 85(2):265–298, Feb. 1997.

[80] "Commitiees of the international committee for information technology standards," available online `http://www.incits.org/committees/`, accessed 2013-08-12.

[81] "List of standard documents defining fibre channel," available online `http://www.t11.org/t11/stat.nsf/v2t?OpenForm&ent=26`, accessed 2013-09-11.

[82] "Fibre channel physical interface-6 rev 0.03 INCITS working draft proposed american national standard for information technology," available online `www.t11.org/ftp/t11/pub/fc/pi-6/13-135v0.pdf`, accessed 2013-09-11, 2013.

[83] "Inifiniband trade association," available online: `http://www.infinibandta.org/`, accessed 2013-08-20.

[84] *InfiniBandTM Architecture Specification Volume 2 Release 1.3*. 2012.

[85] "Micropod^{TM} optical transmitter and receiver modules," available online `http://www.avagotech.com/pages/en/press/micropod` accessed 2013-09-30.

[86] L. Schares, D. M. Kuchta, and A. F. Benner, "Optics in future data center networks," in *Proc. HOTI*, pages 104–108, Aug. 2010.

[87] J. D. Ingham, R. V. Penty, and I. H. White, "10 Gb/s transmitter-based equalization for extended-reach multimode-fiber datacommunication links," in *Proc. OFC*, paper OTuL4, Mar. 2007.

[88] J. D. Ingham, R. V. Penty, and I. H. White, "10 Gb/s & 20 Gb/s extended-reach multimode-fiber datacommunication links using multilevel modulation and transmitter-based equalization," in *Proc. OFC*, paper OTuO7, Feb. 2008.

[89] I. H. White, J. D. Ingham, and R. V. Penty, "Systems aspects of optical technologies for use in datacommunications," in *Proc. OFC*, paper OMM1, Mar. 2011.

[90] "Q:active active copper cables," available online `http://www.intersil.com/signalintegrity/ActiveCables.asp` accessed 2013-08-30.

[91] M. Tavan, E. Agrell, and J. Karout, "Bandlimited intensity modulation," *IEEE Trans. Commun.*, 60(11):3429–3439, 2012.

[92] J. D. Ingham, R. V. Penty, I. H. White, and D. G. Cunningham, "Carrierless amplitude and phase modulation for low-cost, high-spectral-efficiency optical datacommunication links," in *Proc. CLEO*, paper CThC5, 2010.

[93] J. D. Ingham, R. V. Penty, I. H. White, and D. G. Cunningham, "40 Gb/s carrierless amplitude and phase modulation for low-cost optical datacommunication links," in *Proc. OFC*, paper OThZ3, Mar. 2011.

[94] M. I. Olmedo, Z. Tianjian, J. B. Jensen, Z. Qiwen, X. Xu, and I. T. Monroy, "Towards 400 GBASE 4-lane solution using direct detection of multiCAP signal in 14 GHz bandwidth per lane," in *Proc. OFC*, paper PDP5C.10, 2013.

[95] J. Zhang, J. Yu, F. Li, N. Chi, Z. Dong, and X. Li, "11 × 5 × 9.3 Gb/s WDM-CAP-PON based on optical single-side band multi-level multi-band carrier-less amplitude and phase modulation with direct detection," *Opt. Express*, 21(16):18842–18848, Aug 2013.

[96] G.-H. Im and J.-J. Werner, "Bandwidth-efficient digital transmission over unshielded twisted-pair wiring," *IEEE J. Sel. Areas Commun.*, 13(9):1643–1–655, 1995.

[97] S. Walklin and J. Conradi, "Multilevel signaling for increasing the reach of 10 Gb/s lightwave systems," *IEEE J. Lightw. Technol.*, 17(11):2235–2248, Nov. 1999.

[98] J. K. Pollard, "Multilevel data communication over optical fibre," *IEE P-COMMUN*, 138(3):162–168, Jun. 1991.

[99] J. L. Zerbe, C. W. Werner, V. Stojanovic, F. Chen, J. Wei, G. Tsang, D. Kim, W. F. Stonecypher, A. Ho, T. P. Thrush, R. T. Kollipara, M. A. Horowitz, and K. S. Donnelly, "Equalization and clock recovery for a 2.5-10-Gb/s 2-PAM/4-PAM backplane transceiver cell," *IEEE J. Solid-St. Circ.*, 38(12):2121–2130, Dec. 2003.

[100] F. Breyer, S. C. J. Lee, S. Randel, and N. Hanik, "Comparison of OOK- and PAM-4 modulation for 10 Gbit/s transmission over up to 300 m polymer optical fiber," in *Proc. OFC*, paper OWR2, Feb. 2008.

[101] F. Breyer, S. C. J. Lee, S. Randel, and N. Hani, "PAM-4 signalling for gigabit transmission over standard step-index plastic optical fibre using light emitting diodes," in *Proc. ECOC*, paper We.2.A.3, Sept. 2008.

[102] J. E. Cunningham, D. Beckman, X. Zheng, D. Huang, T. Sze, and A. V. Krishnamoorthy, "PAM-4 signaling over VCSELs with 0.13 µm CMOS chip technology," *Opt. Express*, 14(25):12028–12038, Dec. 2006.

[103] J. D. Ingham, R. V. Penty, I. H. White, P. Westbergh, J. S. Gustavsson, Å. Haglund, and A. Larsson, "32 Gb/s multilevel modulation of an 850 nm VCSEL for next-generation datacommunication standards," in *Proc. CLEO*, paper CWJ2, May 2011.

[104] J. Gimlett and N. Cheung, "Dispersion penalty analysis for LED/single-mode fiber transmission systems," *IEEE J. Lightw. Technol.*, 4(9):1381–1392, Sept. 1986.

[105] D. Cunningham, M. Nowell, D. Hanson, and L. Kazovsky, "The IEEE 802.3z worst case link model for optical physical media dependent specification," available online `http://www.ieee802.org/3/z/public/presentations/mar1997/DCwpaper.pdf` accessed 2013-08-06.

[106] "IEEE 802.3ae 10G Ethernet optical link budget spreadsheet," available online `http://ieee802.org/3/10G_study/public/email_attach/All_1250v2.xls` accessed 2013-08-06.

[107] T. Toifl, C. Menolfi, M. Ruegg, R. Reutemann, P. Buchmann, M. Kossel, T. Morf, J. Weiss, and M. L. Schmatz, "A 22 Gb/s PAM-4 receiver in 90-nm CMOS SOI technology," *IEEE J. Solid-State Circuits*, 41(4):954–965, Apr. 2006.

[108] T. E. Darcie, "Subcarrier multiplexing for lightwave networks and video distribution systems," *IEEE J. Sel. Areas Commun.*, 8(7):1240–1248, Sept. 1990.

[109] R. Olshansky, V. A. Lanzisera, and P. M. Hill, "Subcarrier multiplexed lightwave systems for broad-band distribution," *IEEE J. Lightw. Technol.*, 7(9):1329–1342, Sep. 1989.

[110] S. Hranilovič and D. A. Johns, "A multilevel modulation scheme for high-speed wireless infrared communications," in *Proc. ISCAS*, volume 6, pages 338–341, Jul. 1999.

[111] A. O. Wiberg, B. E. Olsson, and P. A. Andrekson, "Single cycle subcarrier modulation," in *Proc. OFC*, Mar. 2009.

[112] B. E. Olsson and M. Sköld, "QPSK transmitter based on optical amplitude modulation of electrically generated QPSK signal," in *Proc. ACP*, Oct. 2008.

[113] B.-E. Olsson and A. Alping, "Electro-optical subcarrier modulation transmitter for 100 GbE DWDM transport," in *Proc. ACP*, paper SaF3, Oct. 2008.

[114] S. Randel, F. Breyer, and S. C. J. Lee, "High-speed transmission over multimode optical fibers," in *Proc. OFC*, paper OWR2, Feb. 2008.

[115] T.-T. Pham, R. Rodes, J. Estaran, J. B. Jensen, and I. T. Monroy, "Half-cycle modulation for VCSEL based 6-Gbaud 4-QAM transmission over 1 km multimode fibre link," *Electron. Lett.*, 48(17):1074–1076, 2012.

[116] T.-T. Pham, R. Rodes, J. B. Jensen, C. J. Chang-Hasnain, and I. T. Monroy, "Half-cycle QAM modulation for VCSEL-based optical links," in *Proc. ECOC*, paper Mo.1.B.3, 2012.

[117] T.-T. Pham, R. Rodes, J. B. Jensen, C. J. Chang-Hasnain, and I. T. Monroy, "Sub-cycle QAM modulation for VCSEL-based optical fiber links," *Opt. Express*, 21(2):1830–1839, Jan 2013.

[118] A. S. Karar and J. C. Cartledge, "Generation and detection of a 56 Gb/s signal using a DML and half-cycle 16-QAM Nyquist-SCM," *Photonics Technology Letters, IEEE*, 25(8):757–760, 2013.

[119] A. S. Karar and J. C. Cartledge, "Generation and detection of a 112-Gb/s dual polarization signal using a directly modulated laser and half-cycle 16-QAM Nyquist-subcarrier-modulation," in *Proc. ECOC*, paper Th.3.A.4, 2012.

[120] A. S. Karar and J. C. Cartledge, "Electronic post-compensation of dispersion for DML systems using SCM and direct detection," *IEEE Photon. Technol. Lett.*, 25(9):825–828, 2013.

[121] J. Armstrong, "OFDM for optical communications," *IEEE J. Lightw. Technol.*, 27(3):189–204, Feb. 2009.

[122] J. S. Chow, J. C. Tu, and J. M. Cioffi, "A discrete multitone transceiver system for HDSL applications," *IEEE J. Sel. Area. Comm.*, 9(6):895–908, Aug. 1991.

[123] J. A. C. Bingham, "Multicarrier modulation for data transmission: an idea whose time has come," *IEEE Commun. Mag.*, 28(5):5–14, May 1990.

[124] S. C. J. Lee, F. Breyer, S. Randel, H. P. A. van den Boom, and A. M. J. Koonen, "High-speed transmission over multimode fiber using discrete multitone modulation (invited)," *J. Opt. Netw.*, 7(2):183–196, Feb. 2008.

[125] S. C. J. Lee, F. Breyer, S. Randel, D. Cardenas, H. P. A. van den Boom, and A. M. J. Koonen, "Discrete multitone modulation for high-speed data transmission over multimode fibers using 850-nm VCSEL," in *Proc. OFC*, paper OWM2, Mar. 2009.

[126] Y. H., S. C. J. Lee, E. Tangdiongga, C. Okonkwo, H. P. A. van den Boom, F. Breyer, S. Randel, and A. M. J. Koonen, "47.4 Gb/s transmission over 100 m graded-index plastic optical fiber based on rate-adaptive discrete multitone modulation," *IEEE J. Lightw. Technol.*, 28(4):352–359, Feb. 2010.

[127] R. You and J. M. Kahn, "Average power reduction techniques for multiple-subcarrier intensity-modulated optical signals," *IEEE Trans. Commun.*, 49(12):2164–2171, Dec. 2001.

[128] W. Kang and S. Hranilovič, "Optical power reduction for multiple-subcarrier modulated indoor wireless optical channels," in *Proc. ICC*, volume 6, pages 2743–2748, Jun. 2006.

[129] S. Randel, F. Breyer, S. C. J. Lee, and J. W. Walewski, "Advanced modulation schemes for short-range optical communications," *IEEE J. Sel. Topics Quantum Electron.*, 16(5):1280–1289, Sept.-Oct. 2010.

[130] E. Hugues-Salas, X. Q. Jin, R. P. Giddings, J. L. Wei, C. Shu, and J. M. Tang, "First experimental demonstration of VCSEL-based realtime end-to-end 11.25 Gb/s optical OFDM signal transmission over 800m MMFs," in *Proc. ECOC*, paper Tu3C1, Sep. 2011.

[131] S. Hranilovič. *Wireless optical communication systems*. Springer Verlag, 2005.

[132] J. Karout, E. Agrell, and M. Karlsson, "Power efficient subcarrier modulation for intensity modulated channels," *Opt. Express*, 18(17):17913–17921, Aug. 2010.

[133] H.-Y. Chen, C.-H. Lin, and S.-J. Jou, "Low-jitter transmission code for 4-PAM signaling in serial links," in *Proc. APASIC*, pages 334–337, 2004.

[134] T. Kibler, S. Poferl, G. Bock, H.-P. Huber, and E. Zeeb, "Optical data buses for automotive applications," *IEEE J. Lightw. Technol.*, 22(9):2184–2199, Sept. 2004.

[135] J.-G. Zhang, "New optical fiber data buses for avionics applications," in *Proc. DASC*, pages 417–422, Oct. 1992.

[136] H. Elgala, R. Mesleh, and H. Haas, "Indoor broadcasting via white LEDs and OFDM," *IEEE Trans. Consum. Electron.*, 55(3):1127–1134, Aug. 2009.